


Sequence and functional differences in the ATPase domains of CHD3 and SNF2H promise potential for selective regulability and drugability

Helen Hoffmeister¹, Andreas Fuchs¹, Elizabeth Komives², Regina Groebner-Ferreira¹, Laura Strobl¹, Julian Nazet³, Leonhard Heizinger³, Rainer Merkl³, Stefan Dove⁴ and Gernot Längst¹ 

¹ Department of Biochemistry, Genetics and Microbiology, Biochemistry III, University of Regensburg, Germany

² Department of Chemistry and Biochemistry, University of California San Diego, La Jolla, CA, USA

³ Department of Biochemistry II, University of Regensburg, Germany

⁴ Department of Pharmaceutical and Medical Chemistry II, University of Regensburg, Germany

Keywords

ADP; ATPase; chromatin; competitive inhibitor; remodeling enzyme

Correspondence

H. Hoffmeister and G. Längst, Department of Biochemistry, Genetics and Microbiology, Biochemistry III, University of Regensburg, Germany

Tel: +49 941 943 1848 (HH); +49 941 943 2849 (GL)

Emails: Helen.Hoffmeister@vkl.uni-regensburg.de (HH),

Gernot.Laengst@vkl.uni-regensburg.de (GL)

(Received 14 July 2020, revised 19 November 2020, accepted 4 January 2021)

doi:10.1111/febs.15699

Chromatin remodelers use the energy of ATP hydrolysis to regulate chromatin dynamics. Their impact for development and disease requires strict enzymatic control. Here, we address the differential regulability of the ATPase domain of hSNF2H and hCHD3, exhibiting similar substrate affinities and enzymatic activities. Both enzymes are comparably strongly inhibited in their ATP hydrolysis activity by the competitive ATPase inhibitor ADP. However, the nucleosome remodeling activity of SNF2H is more strongly affected than that of CHD3. Beside ADP, also IP₆ inhibits the nucleosome translocation of both enzymes to varying degrees, following a competitive inhibition mode at CHD3, but not at SNF2H. Our observations are further substantiated by mutating conserved Q- and K-residues of ATPase domain motifs. The variants still bind both substrates and exhibit a wild-type similar, basal ATP hydrolysis. Apart from three CHD3 variants, none of the variants can translocate nucleosomes, suggesting for the first time that the basal ATPase activity of CHD3 is sufficient for nucleosome remodeling. Together with the ADP data, our results propose a more efficient coupling of ATP hydrolysis and remodeling in CHD3. This aspect correlates with findings that CHD3 nucleosome translocation is visible at much lower ATP concentrations than SNF2H. We propose sequence differences between the ATPase domains of both enzymes as an explanation for the functional differences and suggest that aa interactions, including the conserved Q- and K-residues distinctly regulate ATPase-dependent functions of both proteins. Our data emphasize the benefits of remodeler ATPase domains for selective drugability and/or regulability of chromatin dynamics.

Introduction

In order to regulate DNA accessibility in chromatin for nuclear processes like for example transcription or

replication, cells make use of chromatin modifications such as post-translational modification of histones,

Abbreviations

aa, amino acid; ADP, adenosine diphosphate; ATP, adenosine triphosphate; BRG1, Brahma Related Gene 1; CHD3, Chromodomain Helicase DNA Binding Protein 3; Da, Dalton; EC₅₀-value, Half maximal effective concentration; IC₅₀-value, half maximal inhibitory concentration; IP₆, Inositol hexakisphosphate; ISWI, imitation SWItch; kDa, kilo Dalton; K_d, value (dissociation constant); K_{mapp}, value (apparent Michaelis constant); SNF2H, Sucrose Nonfermenting 2 Homolog; SWI/SNF, SWItch/Sucrose Non-Fermentable.

DNA modification(s), or chromatin-associated RNAs [1–4]. In addition, there are chromatin remodeling enzymes, which act in large multiprotein complexes of two to fourteen proteins. Using a bipartite ATPase domain, these enzymes hydrolyze ATP to provide the energy necessary for altering chromatin structure and DNA accessibility by repositioning or unwrapping nucleosomes, or by exchanging histone molecules [5]. The human genome encodes for 53 ATP-dependent remodeling enzymes, which are in turn classified in 24 subfamilies, all belonging to the Snf2 family of SF2 helicases [6].

Many chromatin remodelers are functionally linked with organismal development or diseases such as cancer [7–11]. Overall, 36.5% of serous tumors exhibit mutations in the genes of chromatin remodeling enzymes [12]. In the case of SNF2H (= SMARCA5; Iswi subfamily) high levels of SNF2H transcripts have been observed in AML (= acute myeloid leukemia) blast cells and in CD34+ hematopoietic progenitors of AML patients [13,14]. Furthermore, SNF2H expression levels have been shown to be increased in HCC (= hepatocellular carcinoma) tissues in comparison with paratumoral liver tissues [15]. Mutations in CHD3 (= MI-2-alpha; Mi-2 subfamily) drive uterine corpus endometrioid carcinoma progression (<https://www.intogen.org/search?gene=CHD3>), and CHD3 has been the most commonly deleted gene, of the existing nine CHD members, across 32 analyzed tumor types, including breast cancer [16].

Due to their important role in organizing chromatin structure, it can be envisioned that these enzymes are subject to a strict regulation by posttranslational modifications and/or binding partners. For dMI-2 (Mi-2 subfamily), it has been proposed that dCK2 constitutively phosphorylates the N-terminus *in vivo* [17]. Interestingly, the dephosphorylation of this region increases the affinity of MI-2 for the nucleosome, stimulating in turn its ATPase- and nucleosome remodeling activity [17]. Furthermore, *in vitro* experiments have shown that acetylation of histone H4 at lysine residue K16 stimulates nucleosome remodeling by dISWI (Iswi subfamily) under certain conditions [18], whereas ACF, a complex of ISWI and ACF1 [19], exhibits different nucleosome positioning properties than dISWI alone [20]. Finally, the depletion or inactivation of mCHD3 at DSB (= double strand break) sites has been suggested to depend on the phosphorylation of the C-terminus of KAP-1, thereby inhibiting the interaction between the SUMO interacting motif (SIM) of CHD3 with SUMO1-conjugated KAP-1 [21].

Beyond that and in regard to the mentioned disease implication, enzymatic regulation is also conceivable

via ligands. As chromatin remodelers possess subfamily-specific domains besides the motor domain (ATPase domain) [6], all those domains would represent promising drug targets. Indeed, PFI-3 has been evaluated as a selective and potent bromodomain inhibitor of BRG1 (= SMARCA4; Snf2 subfamily) [22,23]. Even though many domains have been already well characterized regarding functional aspects [5,24], the development of domain-specific drugs is hampered by the lack of high-resolution structural data [25,26]. In contrast to this, several 3D structures of the ATPase domain of remodelers or SF2 helicases have been published [27–32]. Finally, however, bromodomain function of SMARCA4 has even been shown to be insubstantial for tumor cell proliferation, while the ATPase activity has been crucial [23]. Moreover, the ATPase domain represents the core functional domain of these enzymes, even hosting an autonomous nucleosome translocation module for ISWI [25,30,33,34]. We have therefore assumed that the ATPase domain of remodelers might be a promising target for drugs.

We have performed kinetic and HDXMS (= Hydrogen-Deuterium Exchange Mass Spectrometry) experiments that evidence the competitive ATPase domain inhibition by ADP of human CHD3 (Mi-2 subfamily) and SNF2H (Iswi subfamily), resulting in IC₅₀ values of around 56 μM for both enzymes, regarding ATP hydrolysis. However, somewhat unexpected, the nucleosome translocation ability of CHD3 is less drastically reduced than in SNF2H. In addition to ADP, ATP hydrolysis of both enzymes is inhibited by further nucleotide analogues such as ATPγS or ADPβS, with SNF2H reacting 4 times more sensitively than CHD3 toward ADPβS. Beside ADP, also IP₆ has turned out to inhibit the nucleosome translocation activity of both enzymes to varying degrees, thereby following a competitive inhibition mode at CHD3, but surprisingly not at SNF2H. Overall, our data point to functional differences in the ATPase domains and in ATPase-dependent functions of both remodeling enzymes, which in turn shows the possibility of selectively regulating these enzymes *in vivo* and thus fine-tuning chromatin dynamics according to physiological circumstances. Our experimental data are further substantiated by point mutations of highly conserved Q- and K-residues in the Q- and I-motif of the ATPase domain [11]. All mutants (6 mutants each for CHD3 and 7 for SNF2H) are able to bind nucleosomes and exhibit wild-type similar basal (nonstimulated) ATPase rates, but fail to increase the ATP hydrolysis rates in the presence of nucleosomes, resulting in a general nucleosome remodeling deficiency of the mutants. Notably, three CHD3 mutants (Q740E/A; K767R) compared to only one

cancer-associated SNF2H (D182N) Q-motif mutant can still translocate nucleosomes. In combination with our remodeling results in the presence of ADP, our data therefore argue for the ability to ‘couple’ ATP hydrolysis and nucleosome remodeling more efficiently in CHD3, than in SNF2H. This aspect is supported by findings that despite comparable substrate affinities and ATP hydrolysis parameters, CHD3 nucleosome translocation is visible at much lower ATP concentrations than SNF2H. We propose that the observed functional divergences between CHD3 and SNF2H can be attributed to minor, but characteristic sequence differences between the ATPase domains of both enzymes, which are substantiated by *in silico* sequence comparisons and homology models. We suggest that amino acid interactions, including the conserved Q- and K-residues, distinctly regulate ATPase-dependent functions of both proteins, causing the observed functional differences. In conclusion, our data emphasize the potential of the ATPase domain for selective regulation and/or drug targeting of chromatin remodelers.

Results

The ATPase domains of CHD3 and SNF2H exhibit minor, but characteristic differences

In order to assess whether the ATPase domain of chromatin remodelers represents a promising target for selective inhibitors, we have performed a comprehensive sequence analysis, comparing the ATP-binding domain of representatives from two different subfamilies, namely CHD3 [Mi-2] and SNF2H [Iswi] (Fig. 1A) [6]. Two sequence sets, consisting of 275 (CHD3) and 194 (SNF2H) UniRef 90% sequences, have been compiled. The Q- and I-motif of the ATP-binding domain, being discussed in context of nucleotide binding and/or hydrolysis in SF2 helicases [35–37], are in close proximity to the bound nucleotide in CHD3 (see also below). Remodeler-specific sequence logos substantiate the strict conservation of the full I-motif and of key residues, belonging to the Q-motif (Fig. 1B) [6]. Most

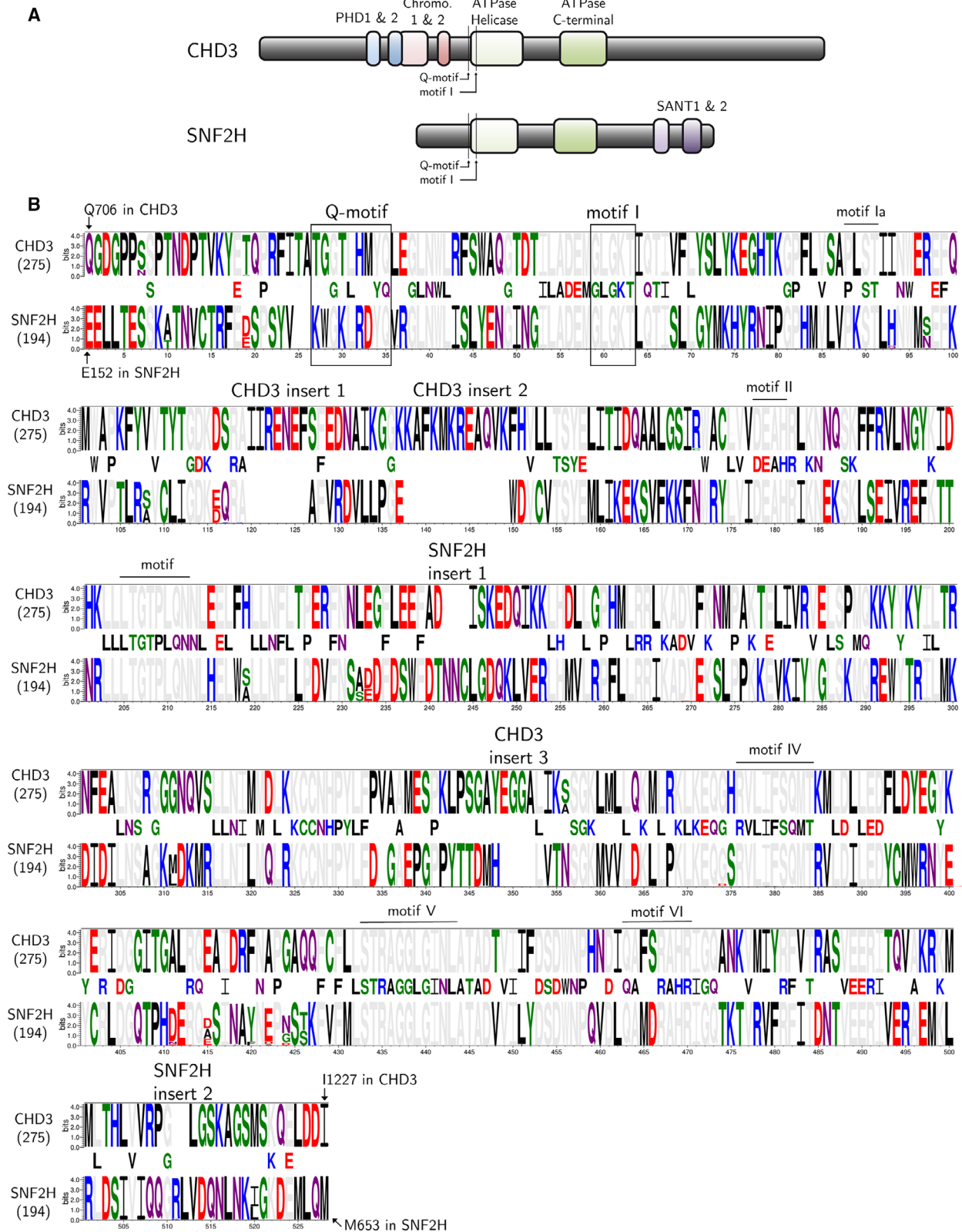
importantly, the Q740/184 (CHD3/SNF2H) and K767/211 (CHD3/SNF2H) residues are strictly conserved in all sequences.

However, in addition to these highly conserved regions, the ATPase domains of both enzymes exhibit less conserved sequence elements, specific for the respective remodeler (Fig. 1B). There are for example three sequence insertions of four and more amino acids in CHD3, which do not exist in SNF2H and as well two smaller amino acid insertions (two and three aa) in SNF2H, which we do not find in CHD3 (Fig. 1B and Fig. S1, Fig. 2). This has prompted us to further assess the suitability of this domain as selective drug target by subjecting hCHD3 and hSNF2H to a detailed comparative, experimental study.

CHD3 and SNF2H display comparable substrate affinities and ATP hydrolysis parameters, but differ in the enzymatic processing power regarding nucleosome translocation

To start with, we have thoroughly characterized and compared both enzymes in regard to ATPase-dependent functions and substrate affinities (Fig. 2 and Fig. S3). In order to analyze the binding parameters of CHD3 and SNF2H for nucleosomes, interaction analyses with fluorescently labeled 0-NPS-0 (= ‘linker-free’) nucleosomes have been performed. The use of such kind of nucleosomes allows to neglect the influence of nucleosome-associated linker DNA, serving as a preferential binding platform for chromatin remodelers (Fig. 2A, decrease of free DNA signal with raising remodeler amounts). We can show that CHD3 and SNF2H have comparable nucleosome binding affinities, ranging within EC_{50} values of 147 ± 27.6 nM (CHD3) and 219 ± 48.1 nM (SNF2H) (Fig. 2A and Fig. S3a). Furthermore, determination of K_d values for the second substrate ATP reveal that CHD3 (i) and SNF2H (ii) also exhibit similar affinities of $440 \mu\text{M}$ (± 213) (i) and $238 \mu\text{M}$ (± 93) (ii) (Fig. 2B and Fig. S3b). Since we have performed our substrate binding assays in the absence of the respective other

Fig. 1. Domain composition of the two human SF2 helicases CHD3 and SNF2H and sequence comparison of their ATPase domains. (A) Schematic representation of CHD3 and SNF2H domains and features. Additionally, localization of the Q-motif and motif I is indicated. (B) Differential logo of chromatin remodeler amino acid regions, containing the ATPase domains of CHD3 (hCHD3: aa 706–1227) and SNF2H (hSNF2H: aa 152–653). The logo is based on a MSA deduced from 275 CHD3 and 194 SNF2H sequences taken from two UniRef 90 clusters. The center line shows residues strictly conserved in both domains, the logos above and below indicate the remodeler-specific composition of sequences. The position of the Q-motif and motif I [6,11] is indicated by a box. The remaining, also highly conserved Walker-motifs [84,6] or sequence specific CHD3 or SNF2H inserts are indicated with black lines. The color code represents the chemistry of the residues. The MSA data set is available in Fig. S2.



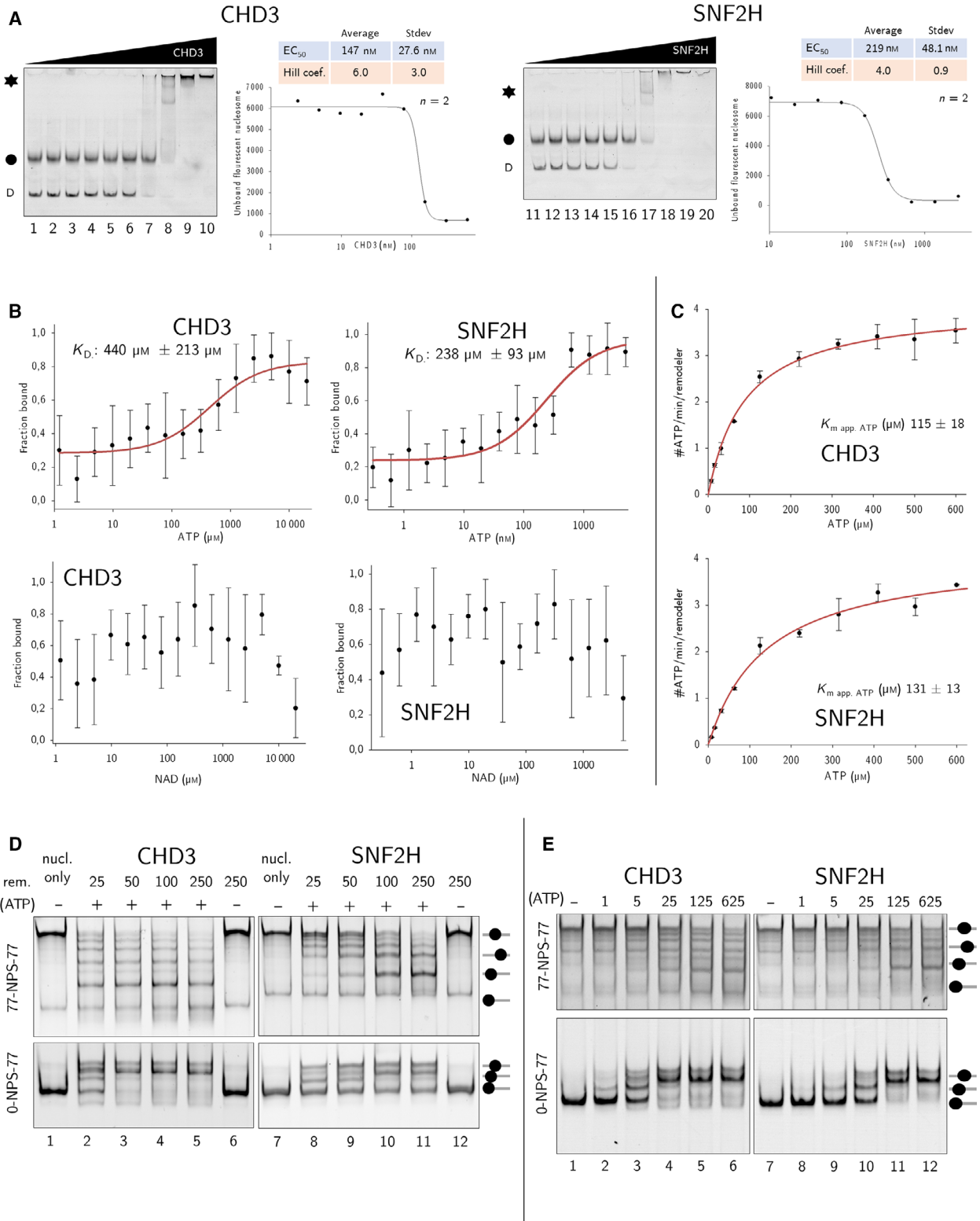


Fig. 2. Comparative analysis of substrate affinities and enzymatic activities of CHD3 and SNF2H. (A) Quantification of binding affinities for human CHD3 and SNF2H for binding to Cy3 labeled 0-NPS-0 mononucleosomes via EMSA (see also Materials and Methods). The EC_{50} values in the colored table derive from 2 independent experiments with two different protein and nucleosome preparations (see also Fig. S3A). The tables are embedded in a diagram, representing the quantification of the corresponding, pictured EMSA experiment (30.2 nM Cy3-labeled 0-NPS-0 mononucleosomes, which were incubated with raising amounts (1 : 2 dilution) of CHD3 (left; highest concentration: 620 nM) and SNF2H (right; highest concentration: 2710 nM). CHD3 first replicate: $EC_{50} = 127$ nM; $n = 8.1$ and SNF2H first replicate: $EC_{50} = 253$ nM; $n = 4.6$. Black asterisk represents shift products; black dot represents 0-NPS-0 nucleosome and D represents free DNA. (B) Raising amounts (1 : 2 dilution) of ATP (upper panel) or NAD (lower panel) were incubated with 25 nM of tris-NTA fluorophore NT647 labeled CHD3-C-His (left; highest ATP/NAD concentration 20 mM) and N-His-SNF2H (right; highest ATP/NAD concentration 5 mM). The experiments were performed at 40% (CHD3) or 80% (SNF2H) MST power. The data were analyzed in the T-Jump mode and fitted to a one-site binding model to determine K_d values. The standard deviation represents $n = 8$ (ATP_CHD3), $n = 6$ (NAD_CHD3), $n = 6$ (ATP_SNF2H), and $n = 6$ (NAD_SNF2H) experiments. Due to its structural similarity to ATP, NAD was selected as negative control. (C) 40 nM CHD3 and 80 nM SNF2H were stimulated with nucleosomes (77-NPS-77), and the ATPase rate was measured for 40 min at 30 °C. ATP was titrated from 8 to 600 μ M. The resulting data were fitted to the Michaelis-Menten equation, to obtain apparent K_m values. The graphs show ATPase rates of a representative experiment, with the calculated apparent K_m values. The standard deviation derives from $n = 6$ (SNF2H) or $n = 5$ (CHD3) independent experiments. (D) 130 nM centrally positioned nucleosomes (77-NPS-77; upper panel) or asymmetrically positioned nucleosomes (0-NPS-77; lower panel) were incubated with 1 mM ATP and the indicated [nM] concentrations of CHD3 (left) and SNF2H (right) for 1 h at 30 °C. Remodeling reactions were analyzed on 6% native PAA gels. (E) 80 nM of 77-NPS-77 (upper panel) and 120 nM of 0-NPS-77 (lower panel) mononucleosomes were incubated with 200 nM remodeling enzyme (left: CHD3; right: SNF2H) at raising ATP [μ M] concentrations (indicated on top of the figure) for 1 h at 30 °C. One reaction served as a control and did not contain ATP. After stopping the reactions, the remodeled nucleosome positions were resolved on 5–6% native PAA gels.

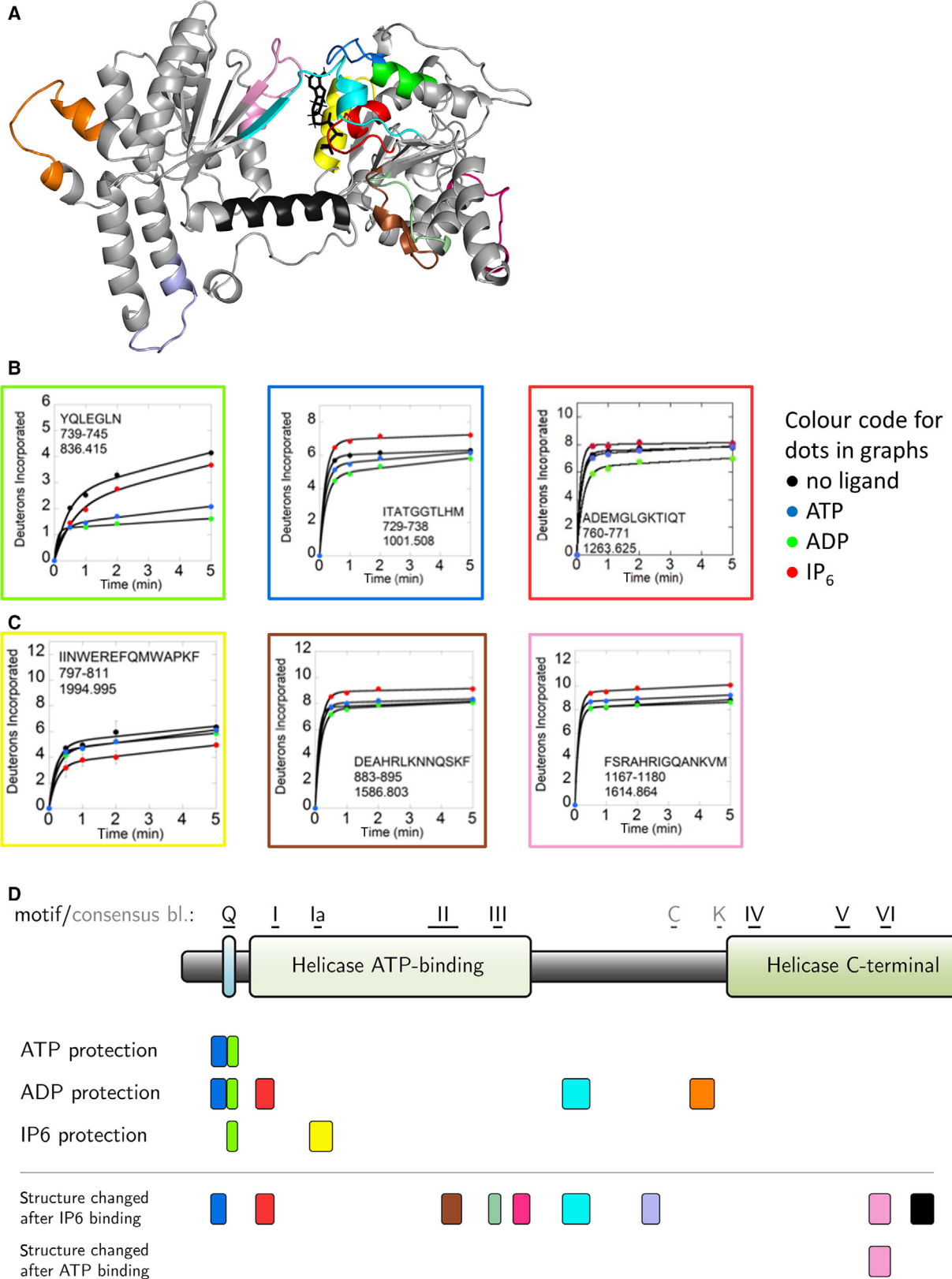
substrate, we can moreover conclude that chromatin remodelers can bind independently to nucleosomes or ATP alone (see also below).

We have next compared CHD3 and SNF2H in (well established) ATP hydrolysis assays, which we have performed in accordance to [38–40]. In a first test, we have titrated ATP from 0 μ M to 600 μ M at a fixed (77-NPS-77) nucleosome concentration of 130 nM (Fig. 2C), ensuring that the hydrolysis rates are linear over the complete ATP concentration range during the assay time (Fig. S3c). Unfortunately, it is not possible to use mononucleosomes at ‘saturating’ concentrations of 2 μ M or higher (see also Fig. 2A) in our assays, since technical limitations (precipitation effects) in the assembly procedure do not allow to achieve nucleosome concentrations of more than 1 μ M. However, free dsDNA or nucleosomal arrays do not represent a satisfying alternative to mononucleosomes, since DNA is known to stimulate recombinant human Mi-2, but not SNF2H [39,41]. However, we can finally show that both enzymes exhibit Michaelis-Menten kinetics under the mentioned, experimental conditions with apparent K_m values of 115 μ M (± 18) for CHD3 and 131 μ M (± 13) for SNF2H (Fig. 2C). Our data are consistent with intracellular ATP concentrations (100 μ M to 10 mM) [42,43] and published K_m values for other chromatin remodeling enzymes such as nucleosome stimulated recombinant Mi-2 with 38 μ M [39], SNF2H (i) and BRG1 (ii) with 37 μ M (± 9) (i) and 200 μ M (± 50) (ii) [41], or yeast SWI/SNF complex with 126 μ M [40]. Furthermore, both enzymes show comparable hydrolysis rates at ATP concentrations of

600 μ M, ranging above the calculated apparent K_m values (Fig. S3d). The latter finding is also reflected by nucleosome translocation assays (Fig. 2D). Taking into account that chromatin remodeling enzymes from different subfamilies exhibit distinct template preferences and nucleosome translocation properties [44], our assays nevertheless allow the conclusion that CHD3 and SNF2H display comparable translocation activities at saturating ATP concentrations of 1 mM ATP on middle (77-NPS-77)- and end (0-NPS-77)-positioned nucleosomes (Fig. 2D and Fig. S3e). Both enzymes are able to move the central nucleosome to the edge of the dsDNA strand (Fig. 2D, upper panel) and vice versa (Fig. 2D, lower panel). However, nucleosome remodeling assays in the presence of rising ATP concentrations (0 to 625 μ M) on different nucleosomal templates reveal that CHD3 already exhibits visible nucleosome translocation activity at lower ATP concentrations in comparison with SNF2H (Fig. 2E and Fig. S3f). Comparing both proteins in different binding and kinetic assays, we can show that they exhibit similar substrate binding and enzymatic properties. Although both proteins show similar ATP hydrolysis activities (Fig. 2C and Fig. S3d), CHD3 seems to be more efficient in coupling ATP hydrolysis to nucleosome mobilization.

ATP and ADP bind in the Q-motif of the ATPase domain

Several ATP-hydrolyzing enzymes are regulated by ADP [43]. We have therefore raised the question,



whether this also applies to chromatin remodeling enzymes, especially since the high degree of structural identity between ADP and ATP would suggest a competitive inhibition mode for ADP.

To start with, we have performed HDXMS experiments in order to examine, whether and if so, in which protein domains of chromatin remodelers ADP can bind (Fig. 3 and Fig. S4). Unfortunately, due to problems with the long-term stability/activity of SNF2H over several days (see also Supplementary Material and Methods: Purification of Flag-tagged and His-tagged remodeling enzymes), we have only been able to perform HDXMS experiments with CHD3. To our knowledge, this is the first presentation of HDXMS studies for such a large protein (2000 aa) (Fig. S4a). The ion mobility separation available on the Synapt G2Si has allowed the detection of 174 peptides that have been observed in all protein samples, providing a high coverage of 62.9% of the CHD3 sequence (Fig. S4a).

Our HDXMS experiments (Fig. 3 and Fig. S4) show that the presence of ATP and ADP provide visible protection in the peptide containing residues 739–745 with the highly conserved Q740 residue of the Q-motif (Fig. 3A,B,D: green and Fig. S4b). The region N-terminal of the conserved Q-residue (residues 729–738) (Fig. 3A,B,D: dark-blue and Fig. S4b) also reveals binding of ATP and ADP, albeit to a lesser extent than residues 739–745. Interestingly, the effects of ADP are more pronounced than those of ATP. Furthermore, several ADP-specific binding sites are detected. Exclusive ADP protection has been observed in the peptide 760–771 that spans the I-motif (Fig. 3A, B,D: red and Fig. S4b). Thus, ATP and ADP bind to the Q-motif and the latter in addition to the I-motif. Both motifs are in close proximity to the bound nucleotide in the homology model of CHD3 (Fig. 3A). Further regions of exclusive ADP protection include residues 965–982 and 1040–1055 (between consensus blocks C and K), which are in the linker region and

distant from the main nucleotide binding pocket (Fig. 3A,D: light-blue and orange, respectively, and Fig. S4b). Interestingly, in addition to the identification of nucleotide binding sites within the ATPase domain, our HDXMS studies also reveal regions of increased deuterium exchange upon ATP binding (Fig. 3A,C,D and Fig. S4b). These include regions within aa 1167–1180 (Fig. 3A,C,D: pink) and C-terminal of the ATPase domain (aa 1318–1333, aa 1375–1400, aa 1968–1978) (Fig. S4b). Increased exchange, caused by binding of a ligand, can only be explained by an allosteric ‘opening’ or increase in dynamics at a region different from the binding region [45].

Finally, we cannot identify additional binding sites for the nucleotides outside of the bipartite ATPase domain. The overlap of ADP and ATP binding sites in the Q-motif of the ATPase domain together with the high structural similarity of both molecules argue in favor of ADP acting as a competitive inhibitor on CHD3. Since both enzymes show a high degree of identity in the ATPase domain (Fig. 1B), it can be assumed that this also applies to SNF2H.

While ADP comparably inhibits the ATP hydrolysis rate of CHD3 and SNF2H, SNF2H-dependent nucleosome remodeling is preferentially inhibited compared to CHD3

To test, whether ATPase-dependent functions CHD3 and SNF2H are inhibitable by ADP, we have performed ATPase assays at fixed ATP concentrations of 125 μM (Fig. 4A), close to the calculated, apparent K_m values (Fig. 2C) of both enzymes (with 77-NPS-77 nucleosomes). This allows a classification of the selectivity of a putative ligand/inhibitor against different enzymes based on its binding affinity for different kinases, as there is a linear correlation between the IC_{50} and ATP concentration for competitive inhibitors (see also Fig. 3 and Fig. S4) according to the Cheng-Prusoff law ($\text{IC}_{50} = K_i + (K_i/K_m \times [\text{ATP}])$) [46]. The

Fig. 3. ADP, ATP, and IP_6 binding profiles in ATPase domain of CHD3. Hydrogen/deuterium exchange mass spectrometry (HDXMS) with CHD3. A final concentration of 5 μM CHD3 was incubated with 1 mM ATP, ADP, or IP_6 . Regions protected by ligands were resolved via MS (see also Material & Methods). (A) Homology model of the CHD3 ATPase domain (amino acids 706 to 1227, done with I-TASSER server/PyMOL v 1.8.0.6 programme, see also Supplementary S10 Material & Methods). The nucleotide binding site and regions with structural changes are colored. The regions in the model in (A) are labeled with the same color code as the frames and boxes in (B), (C), and (D). (B) + (C) Boxes with colored frames show selected graphs, presenting the deuterium uptake within 5 minutes within certain aa regions in the absence or presence of ATP, ADP, and IP_6 . The graphs presented in the colored boxes are discussed in detail in the text. Additional deuterium uptake plots are given in Fig. S4b. The color code of the boxes in (B) and (C) corresponds to the colors used in (A) & (D). (D) Schematic representation of the CHD3 ATPase domain (aa 706–1227). The boxes below the ATPase domain show regions protected (i.e. bound) by ATP, ADP, and IP_6 . Boxes below the horizontal line represent regions with increased deuterium exchange (i.e. structural changes) upon ATP or IP_6 binding. The color code of the boxes in (D) corresponds to the colors used in (A), (B), and (C).

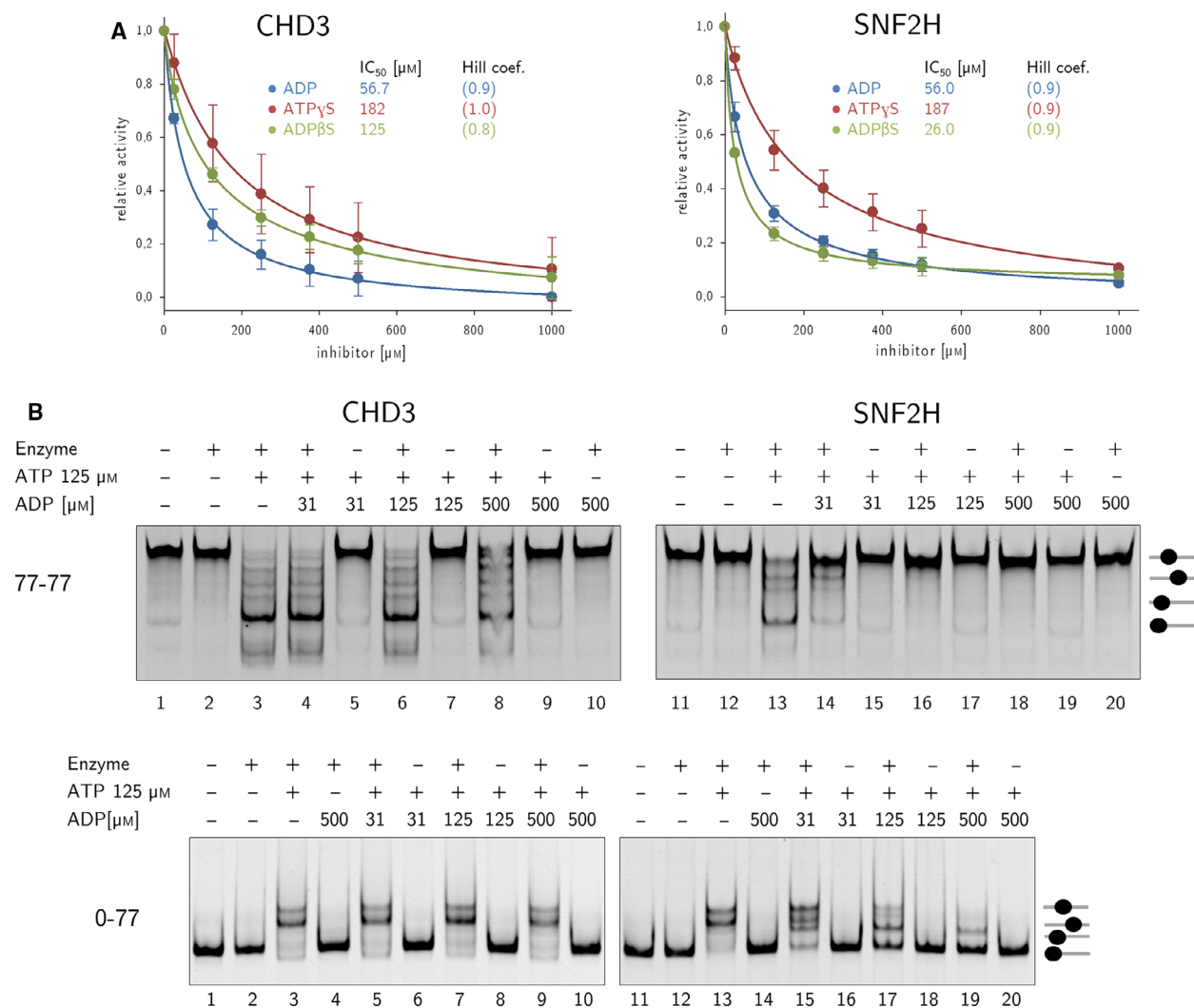


Fig. 4. ATP hydrolysis rates and nucleosome remodeling of CHD3 and SNF2H in the presence of ADP. (A) Chromatin (130 nM 77-NPS-77) stimulated ATPase rate for CHD3 (40 nM) and SNF2H (80 nM) was measured at 30 °C for 40 min, 125 μM ATP and rising concentrations of ADP, ADP β S, or ATP γ S. Data were fitted to the Hill equation, to obtain IC₅₀ values (μM) and a Hill coefficient (n). Data represent $n = 4$ experiments for CHD3 and $n = 3$ experiments for SNF2H. (B) 120 nM of centrally (top: 77-NPS-77) and asymmetrically (bottom: 0-NPS-77) positioned mononucleosomes were incubated with 200 nM remodeling enzyme (left: CHD3; right: SNF2H) at 125 μM ATP and in the absence or presence of ADP (concentrations in μM are indicated on top of the gels) for one hour at 30 °C. After stopping the reactions, the remodeled nucleosome positions were resolved on 5% native PAA gels. The data represent $n = 3$ experiments.

ATP hydrolysis rates of both enzymes decrease with raising ADP concentrations, whereby similar IC₅₀ values of 56.7 (CHD3) and 56 (SNF2H) μM are reached (Fig. 4A and Fig. S5a), which correlate well with physiological concentrations of free ADP in the μM range [42,43,47,48]. Taken together, both enzymes exhibit similar sensitivities for ADP [46] regarding ATP hydrolysis. The calculated Hill coefficients (n) for ADP range around 0.9 (Fig. 4A), arguing for a 1 : 1 binding stoichiometry [46]. Next, we have therefore

tested, whether ADP also inhibits the nucleosome translocation activity of CHD3 and SNF2H. We have performed nucleosome remodeling assays with centrally (77-NPS-77)- and end (0-NPS-77)-positioned nucleosomes at a fixed ATP concentration of 125 μM (around the calculated apparent K_m) and varying ADP concentrations (Fig. 4B). Both remodelers display a visible translocation activity at this ATP concentration, and the reactions are not yet completely ‘end-remodeled’ (Fig. 2E and Fig. S3f). CHD3 efficiently

repositions the nucleosome to the edge of the dsDNA or to the center of the dsDNA fragment (depending on the nucleosome type), even in the presence of a fourfold excess of ADP over ATP, where it starts to show first signs of inhibition (Fig. 4B, upper panel (left): compare lane 3 with 4,6,8; lower panel (left): compare lane 3 with 5,7,9). In contrast, SNF2H behaves differently and is already visibly inhibited at a fourfold deficit for ADP compared with ATP (Fig. 4B, upper panel (right): compare lane 13 with 14,16,18; lower panel: compare lane 13 with 15,17,19). This can be also seen on physiological templates such as drosophila HSP70 promoter or mouse rDNA promoter (Fig. S5b). Taken together, CHD3 and SNF2H are comparably impaired in their ATP hydrolysis rates (Fig. 4A), but the remodeling activity of SNF2H is more affected than that of CHD3 (Fig. 4B and Fig. S5b). The latter observation is also reflected, albeit to a lesser pronounced extent, by remodeling experiments with 77-NPS-77 nucleosomes under saturating substrate concentrations (1 mM ATP) (Fig. S5c). We can see that the remodeling activity of SNF2H decreases in correlation with the increase of ADP and is completely stopped at 3 mM ADP. CHD3, however, shows no significant change in remodeling at ADP concentrations between 250 and 1000 μM . But at 3 mM ADP, it is also nearly completely blocked (Fig. S5c).

To examine whether nucleotides might somehow influence the binding behavior of remodeling enzymes to nucleosomes, we have performed IP experiments with Streptavidin immobilized, biotinylated 77-NPS-77 nucleosomes. Our experiments reveal that the absence or presence of 1 mM ADP or of 1 mM of the nucleotide analogues ATP γ S (nonhydrolysable) or ADP β S (see also below) does not prevent SNF2H and CHD3 from binding to nucleosomes (Fig. S5d). This in turn excludes a significant decrease or loss of nucleosome affinity as an explanation for the differences in remodeling activity in the presence of ADP between SNF2H and CHD3.

A possible explanation for our observations could therefore be a difference in enzymatic processing power, as we have already seen it in Fig. 2E (and Fig. S3f), finally allowing CHD3 to transfer the remaining energy of the impaired ATP hydrolysis more efficiently into the nucleosome translocation process than SNF2H. In addition, they suggest selective regulability of remodeling enzymes, allowing in turn fine regulation of the chromatin structure depending on physiological conditions.

The differential regulation of the two remodelers by ADP suggests that these enzymes may also exhibit different susceptibilities to other nucleotide-based

compounds binding at the ATPase domain. We have therefore tested the inhibitory potential of further nucleotide analogues such as ADP β S and ATP γ S in radioactive ATPase assays (Fig. 4A and Fig. S5a). Just like ADP, ATP γ S and ADP β S reduce the hydrolysis rate of the two enzymes with increasing concentrations (Fig. 4A and Fig. S6a). ATP γ S is the least potent molecule, being reflected by similarly high IC₅₀ values of 182 μM for CHD3 and 187 μM for SNF2H (Fig. 4A). In contrast, ADP β S inhibits SNF2H (i) fourfold more strongly than CHD3 (ii) (IC₅₀ values 26 μM (i) and 125 μM (ii), respectively, see Fig. 4A). The calculated Hill coefficients (*n*) for all three molecules range between 0.8 and 1.0 (Fig. 4A), which (again) speaks more for a 1 : 1 binding stoichiometry than for cooperative effects [46].

In addition, we can show preliminary data for ApCp, exhibiting as well a stronger inhibitory effect on the ATP hydrolysis rate of SNF2H than for CHD3 (Fig. S5a).

ADP inhibits CHD3 and SNF2H in a competitive inhibition mode

Our binding and enzymatic assays show that ADP inhibits both enzymes and binds into the substrate pocket of CHD3, suggesting a competitive inhibition mechanism (Figs 3 and 4). In order to examine the ADP inhibition mode in more detail, we have performed in addition kinetic ATP hydrolysis assays, as presented in Fig. 2C (with 77-NPS-77 nucleosomes). The addition of 10 μM and 20 μM ADP results in increased *K_m* values of both remodelers, without any significant changes in the *V_{max}* values (Fig. 5A), when fitting the curves without constraints. This result again suggests that ADP acts as a competitive inhibitor (Fig. 5A), a finding, which is also supported by nucleosome remodeling assays on centrally (77-NPS-77)- or end (0-NPS-77)-positioned nucleosomes (Fig. 5B/6B). The remodeling assays have been performed according to the experiments presented in Fig. 4B (and Fig. S5b) in the presence of 300 μM or 500 μM ADP, since we can anticipate a visible inhibition effect in the remodeling activity of both enzymes after one hour (and see also Fig. 4A). As expected, the presence of ADP inhibits histone octamer translocation, maintaining nucleosomes rather at the initial (central or edge, depending on the respective nucleosome type) position (Fig. 5B, compare lanes 2/6; 10/14 and Fig. 6B, compare lanes 2/10 and 15/20). The addition of extra ATP after one hour of incubation (Fig. 5B, lanes 8–9; 16–17 and 6b, lanes 12–13; 22–24) enhances the remodeling activity of both remodelers (inhibited and noninhibited,

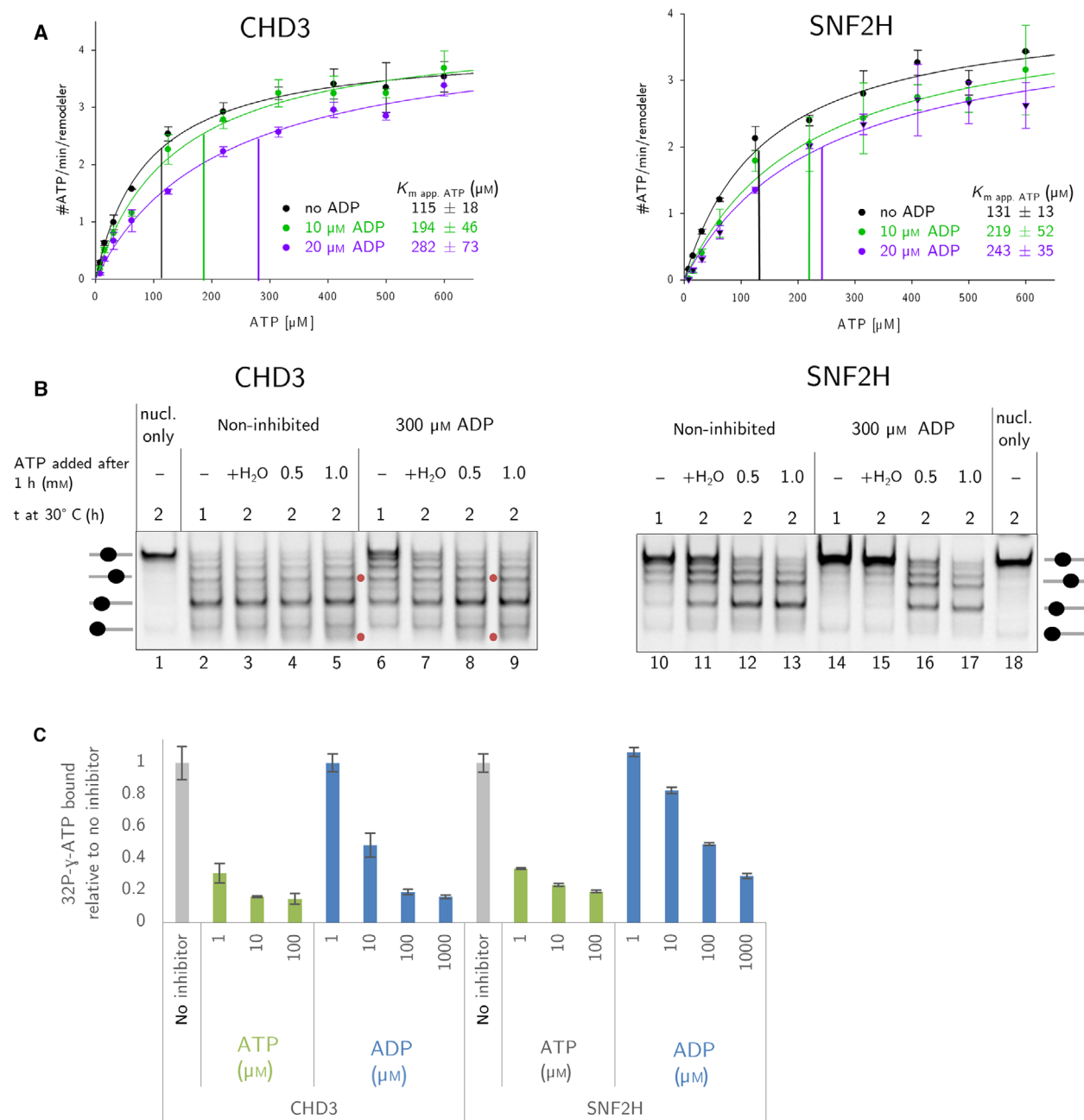


Fig. 5. Experimental analysis of the ADP inhibition mechanism for CHD3 and SNF2H. (A) 40 nM CHD3 and 80 nM SNF2H were stimulated with nucleosomes (77-NPS-77) and the ATPase rate was measured (40 min, 30 °C) in the absence (blue) or presence of 10 μM (green) and 20 μM (violet) ADP. ATP was titrated from 8 to 600 μM . The resulting data were fitted to the Michaelis-Menten equation, to obtain apparent K_m values. The graphs show ATPase rates of a representative experiment, overlaid with the calculated apparent K_m values as colored lines. The standard deviation derives from $n = 6$ (SNF2H) or $n = 5$ (CHD3) independent experiments. The graphs, presenting the noninhibited Michaelis-Menten kinetics for CHD3 and SNF2H are identical with those from Fig. 2C. (B) 200 nM CHD3 and SNF2H were incubated with 120 nM mononucleosomes and 125 μM ATP in the absence or presence of 300 μM ADP (1 h, 30 °C). Reactions were either stopped after 1 h (- ATP: lanes 2, 6, 10, 14) or incubated for a further hour at 30 °C with 0.5 mM ATP (0.5), 1.0 mM ATP (1.0), or water (+ H₂O) [lanes 3–5, 7–9, 11–13, 15–17]. After stopping, the reactions were loaded on a 6% PAA gel to visualize and resolve the remodeled nucleosome positions. The data represent $n = 3$ experiments. (C) 200 nM of proteins was incubated with 0.375 μCi ³²P- γ -ATP and indicated concentrations of nonradioactive ATP or inhibitors (30 min, 30 °C). The reactions were spotted on a nitrocellulose membrane. Bound ³²P- γ -ATP was quantified with a phosphoimager screen. Error bars represent the standard deviation (SD) of three technical replicates.

marked with red dots between lanes 5/6 and 8/9), resulting in a higher fraction of central- or edge-positioned nucleosomes (depending on the respective nucleosome type). The effects caused by the surplus of ATP are higher than the effects of water controls (+ H₂O) carried along. The reversal of ADP inhibition by adding an excess of ATP argues again for a competitive inhibition mode. These observations are in good agreement with data from filter binding assays, which have been performed according to [9,11] (Fig. 5C). Nonradioactive ATP and to a lower extent nonradioactive ADP displace radioactive ATP, being bound to the (filter) immobilized CHD3 and SNF2H proteins (Fig. 5C). In correlation with the HDXMS data, presented in Fig. 3, we suggest that ADP binds to the substrate binding site of CHD3 and SNF2H, which is in accordance with a competitive inhibition mode [46].

IP₆ exhibits distinct inhibition modes for CHD3 and SNF2H

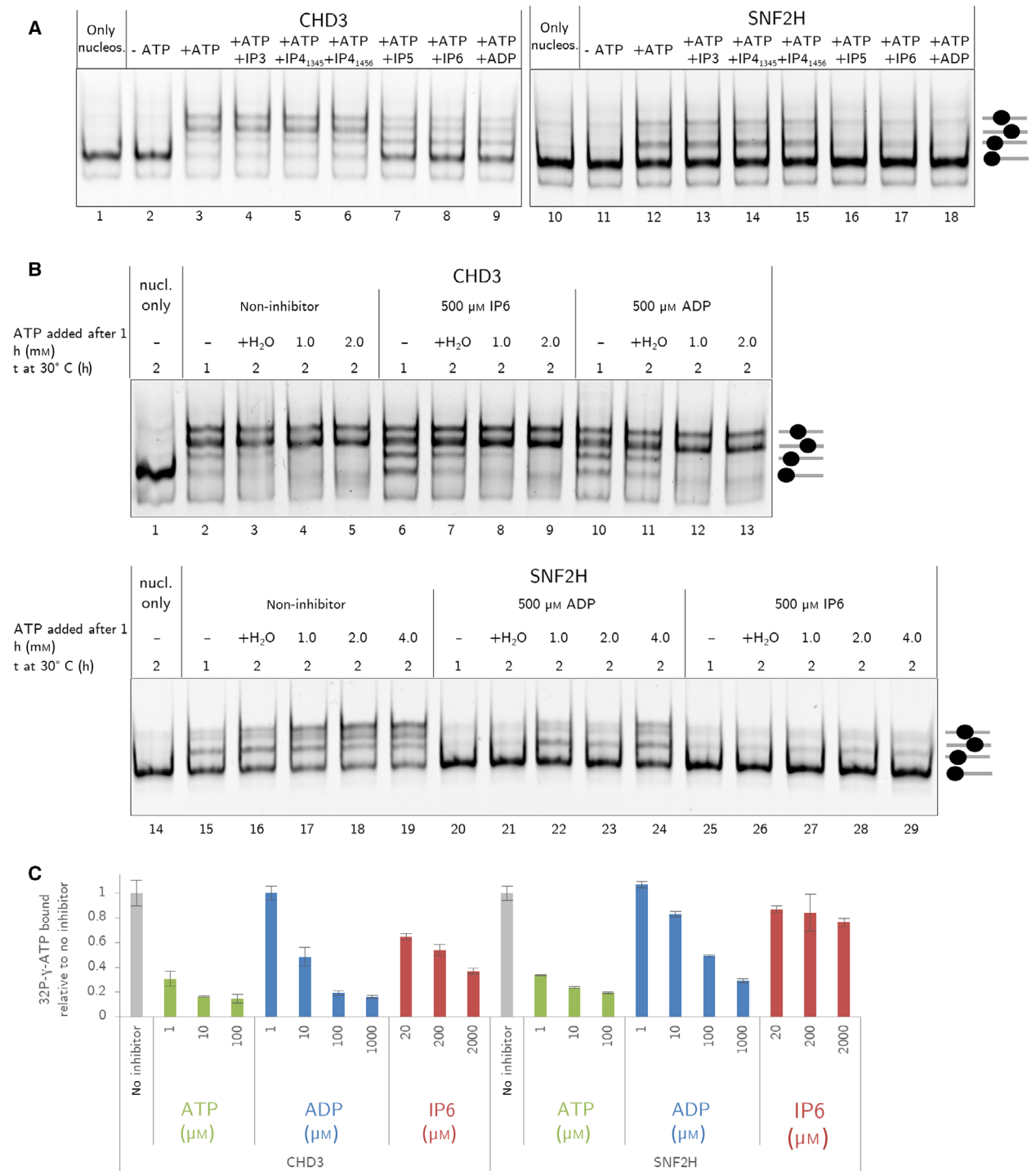
The differential regulation of CHD3 and SNF2H by ADP has made us questioning, whether other cellular signaling molecules would also selectively regulate chromatin remodeling enzymes. IP₆ has been previously shown to regulate rNURF [Iswi subfamily], yISWI2 [Iswi subfamily], SWI/SNF [Snf2 subfamily], INO80 complex [Ino80 subfamily], and hIno80 [Ino80 subfamily] (Fig. S6a) [49–51]. Accordingly, we have tested the family of inositol phosphates, including IP₃, IP_{1,3,4,5}, IP_{1,4,5,6}, IP₅, and IP₆, for their effects on the nucleosome translocation activity of CHD3 and SNF2H on edge (0-NPS-77)- and centrally (77-NPS-77)-positioned nucleosomes, using ADP as a comparative control (Fig. 6A and Fig. S6b). The assays have been performed according to the experiments presented in Fig. 4B (and Fig. S5b) with a fixed concentration of 500 μM IP₆ (or ADP), corresponding to the IP₆ concentration range used in [49,51]. As inositol phosphates might complex the essential magnesium ions [51], we increased the magnesium concentration in our assays to 2.5 mM, allowing efficient nucleosome remodeling without aggregating chromatin [52]. IP₃ and IP_{1,3,4,5} do not affect the enzymatic activities of CHD3 and SNF2H, while IP_{1,4,5,6} exhibits—if at all—only marginal inhibitory effects. However, IP₅ and IP₆ visibly reduce the nucleosome remodeling activity of both enzymes (Fig. 6A and Fig. S6b). Since there are more experimental data available for the direct influence of IP₆ on chromatin remodelers [49,51], we further focus on experiments with IP₆.

IP₆-dependent inhibition of nucleosome translocation is—similar to ADP—more pronounced for

SNF2H than for CHD3 (Fig. 6A,B and Fig. S6b). As shown for ADP and ATPγS, IP₆ does not prevent SNF2H and CHD3 from binding to nucleosomes (Fig. S6c). We have therefore next examined whether IP₆ inhibition can be reverted by rising ATP concentrations in a remodeling assay, as shown in Fig. 5B/6B for ADP (Fig. 6B). As a substrate, we have chosen edge-positioned nucleosomes and IP₆ and ADP (the latter one serving again as a comparative control) have been used at concentrations of 500 μM. Surprisingly, only the remodeling activity of CHD3 is recovered by an excess of ATP. In case of SNF2H, surplus of ATP does not reverse the inhibition even at higher concentrations (Fig. 6B). These results are substantiated by ATP filter binding experiments (Fig. 6C). Similar to nonradioactive ADP, nonradioactive IP₆ displaces radioactive ATP, bound to (filter) immobilized CHD3, albeit with a lower efficiency than ADP (Fig. 6C). In contrast, in case of SNF2H only rising amounts of ADP, but not of IP₆ are capable to compete for the bound radioactive ATP (Fig. 6C). Taken together, our kinetic and binding assays propose a competitive IP₆ inhibition mode for CHD3, but not for SNF2H. The competitive IP₆ inhibitor aspect for CHD3 is further supported by HDXMS experiments (Figure 3 and Figure S4). Our HDXMS experiments (Fig. 3 and Figure S4) show that just like ADP and ATP, IP₆ provides visible protection in the peptide containing residues 739–745 with the highly conserved Q740 residue of the Q-motif (Fig. 3A,B,D: green and Fig. S4b). The effects of IP₆ on this protein region are considerably weaker than those of ATP and ADP. Furthermore, the region comprising residues 797–811, subsequent to motif 1a and adjacent to the predicted nucleotide binding pocket, is exclusively protected by IP₆ (Fig. 3A,C,D: yellow and Fig. S4b).

Finally, no additional binding sites for IP₆ outside of the bipartite ATPase domain of CHD3 have been identified. This finding is in agreement with the competitive binding mode of ADP and IP₆ in CHD3.

Interestingly, in addition to the identification of nucleotide binding sites within the ATPase domain, our HDXMS studies also revealed regions of increased deuterium exchange upon IP₆ binding (Fig. 3A,C,D and Fig. S4b). Regions of increased exchange upon IP₆ binding either include protein domains, where ATP and/or ADP are actually binding (Fig. 3A,B,D: dark-blue, red and light-blue), or novel regions, lacking binding of ATP or ADP (Fig. 3A,C,D: brown, dark pink, gray and black). We also observe regions of increased deuterium exchange, identical for IP₆ and ATP (ATP effects are always weaker) (Fig. 3A,C,D:



pink and Fig. S4b). Our data clearly indicate structural rearrangements of CHD3 upon binding of ATP and IP₆, but not of ADP.

In summary, the experiments suggest a competitive IP₆ inhibition mode for CHD3, but a different model for SNF2H.

Fig. 6. Nucleosome remodeling of CHD3 and SNF2H in the presence of IP₆. (A) 100 nM CHD3 (left) and SNF2H (right) were incubated for 1 h at 30 °C with 130 nM end positioned (0-NPS-77) mononucleosomes, 125 μM ATP, and 500 μM of different inositol phosphates. 500 μM ADP served as positive control for a validated inhibitor (see also Figs 2A and 3B). The data represent *n* = 2 experiments. (B) Remodeling reactions with inhibitors were carried out as in (A). After 1 hour, some samples were stopped (lanes 2, 6, 10, 15, 20, and 25), while others were supplemented with water (+ H₂O) or with 1 (1.0), 2 (2.0), or 4 (4.0) mM ATP (lanes 3–5, 7–9, 11–13, 16–19, 21–24, and 26–29) and incubated for a further hour at 30 °C. After stopping these reactions, all samples were loaded on 6% PAA gels to visualize and resolve the remodeled nucleosome positions. The data represent *n* = 2 experiments. (C) 200 nM of proteins were incubated with 0.375 μCi ³²P-γ-ATP and indicated concentrations of nonradioactive ATP, ADP or IP₆ for 30 min at 30 °C. The reactions were spotted on a nitrocellulose membrane. Bound ³²P-γ-ATP was quantified after exposure on a phosphorimager screen. Error bars represent the standard deviation (SD) of three technical replicates. The values for the titration of nonradioactive ATP and ADP serve as comparative controls and derive from the assay in Fig. 5C.

Three Q- and I-motif variants of CHD3 and only one cancer-associated Q-motif variant of SNF2H are able to translocate nucleosomes

We have demonstrated that various ATPase-dependent processes of CHD3 and SNF2H are differently affected by inhibitors like ADP, ADPβS, and IP₆ (Figs 1–6). Furthermore, we have identified distinct inhibitory modes of IP₆ for CHD3 and SNF2H, respectively. We propose that these differences might be causally linked with sequence differences in the ATPase domain of the two enzymes (Fig. 1B and Fig. S1,2). In order to experimentally address this aspect by another experimental approach, we have performed mutagenesis study on two ATPase domain motifs with documented functional relevance in SF2 helicases [53–55], to compare both enzymes in various ATPase-dependent processes and activities.

We have exchanged the highly conserved Q740/184 (Q-motif: CHD3/SNF2H) and K767/211 (motif I CHD3/SNF2H) residues in the N-terminal part of the ATPase domain with biochemically similar amino acids or alanine in the context of both full-length proteins. Both amino acids belong to motifs, which are in close contact with ADP or ATP according to the HDXMS experiments (Fig. 3 and Fig. S4), and which have been shown to stimulate the ATPase and chromatin remodeling activities of BRG1 upon binding to nucleosomes, probably via allosteric mechanisms [11]. Additionally, we have studied a SNF2H mutant (Q-motif, D182N) being associated with cancer progression (Cosmic database) [56]. We have expressed the proteins in Sf21 cells and have purified them (Fig. S7a/c) in order to compare them in various enzymatic and binding assays (Fig. 7 and Fig. S8/9).

Our filter binding assays reveal that all mutants are still capable of binding ATP (Fig. 7A). These assays do not enable quantitative conclusions [11]. However, since all proteins exhibit ATP signals above the IgG background, which can be competitively displaced by nonradioactive ATP, the results therefore suggest that

all our proteins are able to specifically bind ATP (in the absence of nucleosomes).

Next, we have tested the ATPase activity of the enzymes in the absence and presence of 77-NPS-77 nucleosomes (Fig. 7B). All mutants exhibit a general loss of nucleosome stimulated ATPase activity (Fig. 7B). Surprisingly, the basal (= nonstimulated) ATPase activity of all mutant enzymes is similar to the basal activity of the nonstimulated wild-type enzyme (Fig. 7B), suggesting that none of the mutated amino acids are required for nucleotide binding or basal (= nonstimulated) ATP hydrolysis, but rather for the perception and/or transmission of the nucleosome-dependent stimulation of the ATP hydrolysis rate. These observations are in agreement with findings made for hBRG1 Q- and motif I-mutants [11].

Nucleosome binding assays with biotinylated 77-NPS-77 nucleosomes show that the loss of nucleosome stimulated ATPase activity does not result from the inability of the enzyme variants to bind nucleosomes. Similar to the wild-type proteins, all mutant proteins can still bind centrally positioned nucleosomes (Fig. S8).

Ongoing (basal) ATP hydrolysis and the unaltered ability to bind to nucleosomes have prompted us to test, whether the enzymes are still capable to remodel nucleosomes. We have therefore performed nucleosome translocation assays on central (77-NPS-77)- and edge(0-NPS-77)-positioned nucleosomes in the presence of 1 mM ATP, where both wild-type proteins exhibit a clearly visible nucleosome translocation activity (Fig. 7C, lanes 6/7, 20/21, 35/36, 47/48, and Fig. S9, lanes 6/7, 20/21, 35/36, 47/48, 62/63, 77/78). In correlation with the ATPase assays (Fig. 7B), most of the CHD3 and SNF2H mutants display no detectable remodeling activity on both nucleosome types (Fig. 7C and Fig. S9). However, the K767R, Q740E, and Q740A variants of CHD3 and only the cancer-related SNF2H variant (D182N) are still able to visibly translocate nucleosomes on both nucleosome

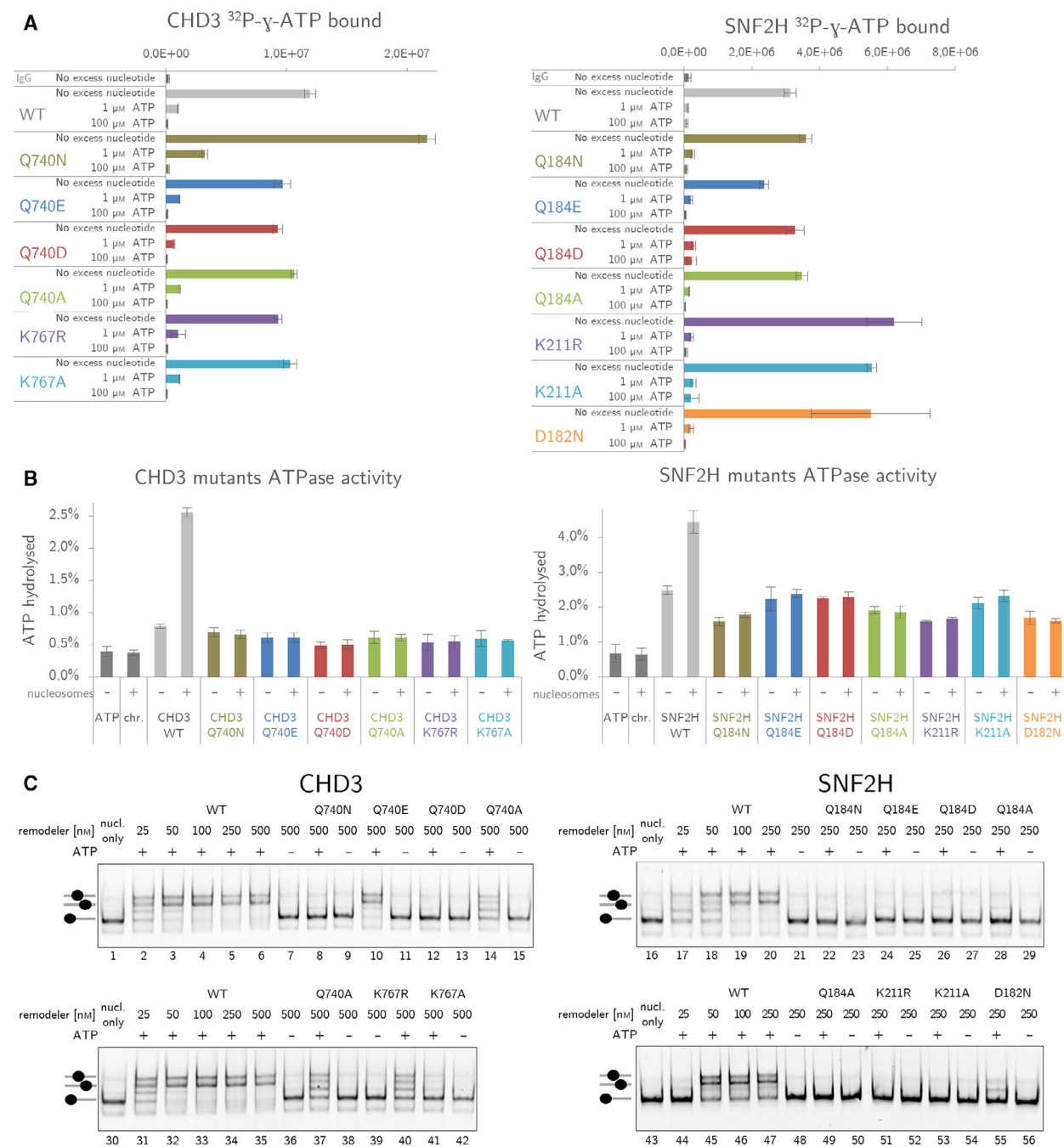


Fig. 7. Comparative functional analysis of the Q-motif and motif I mutants of CHD3 and SNF2H. (A) ATP binding of CHD3 (left), SNF2H (right) and their respective mutants. 200 nM of proteins were incubated with 0.375 μCi ³²P-γ-ATP in the absence or presence of the indicated concentrations (in μM) of nonradioactive ATP. The reactions were spotted on a nitrocellulose membrane. Reactions with 200 nM IgG served as a control. Bound ³²P-γ-ATP was quantified after exposure on a phosphorimager screen. Error bars represent the standard deviation (SD) of three technical replicates. (B) 40 nM CHD3 (left), 80 nM SNF2H (right) and their respective mutants were incubated with 130 nM mid positioned (77-NPS-77) mononucleosomes, 0.1 μCi ³²P-γ-ATP, and 500 μM nonradioactive ATP for 40 min at 30 °C. The data represent *n* = 2 experiments. (C) Chromatin remodeling assays with CHD3, SNF2H, and their respective mutants. Increasing concentrations of WT protein (indicated in the figure in nM) and 250 or 500 nM of the mutant proteins were incubated with 130 nM end positioned (0-NPS-77) mononucleosomes in the absence and presence of 1 mM ATP for 1 h at 30 °C. After stopping the reactions, the remodeled nucleosome positions were resolved on 6% native PAA gels. The data represent *n* = 2 experiments.

templates, albeit with less activity than the respective wild-type protein (Fig. 7C, lanes 10/11, 14/15, 37–40, 55/56, and Fig. S9, lanes 10/11, 14/15, 37–40, 55/56, 70/71, 85/86). Control reactions, containing the same concentration of remodeling enzyme without ATP ensure that the observed nucleosomal band patterning derives from ‘active’, ATP-dependent mechanical nucleosome translocation and not from nonspecific binding events. Finally, our data show that CHD3 is less sensitive to the replacement of both highly conserved and functional relevant amino acids than SNF2H regarding its nucleosome translocation activity. In other words, CHD3 is again more efficient than SNF2H in converting the remaining energy of an impaired ATP hydrolysis (Fig. 7B) into nucleosome translocation. This correlates with the more robust activity of CHD3 in nucleosome remodeling at low ATP concentrations or in the presence of ADP, when compared to SNF2H (Figs 2E, 4B and Fig. S3f, S5b). Beyond that, our CHD3 remodeling data allow the conclusion that the highly conserved Q- and K-residues are not only involved in transmitting nucleosome-dependent stimulation on the ATP hydrolysis rate (see also Fig. 7B), but also in transferring the energy, released from ATP hydrolysis, into the mechanical movement of nucleosomes.

Most plausibly, differing ATPase domain residue interactions, not necessarily restricted, but certainly including the two conserved residues, cause the functional differences observed in the mutants, as well as in CHD3 and SNF2H with respect to ADP, ADP β S, and IP $_6$.

Discussion

We have shown that ADP can competitively inhibit ATP hydrolysis and nucleosome remodeling of CHD3 and SNF2H by binding to the ATPase domain of both enzymes (Figs 3–5 and Figs S4 and S5c). In accordance to this finding, the ATP hydrolysis activity of both remodelers can be inhibited by further nucleotide analogues such as ATP γ S, ADP β S, or ApCp (Fig. 4A and Fig. S5a). Interestingly, both enzymes display different sensitivities toward nucleotide-inhibitors in various ATPase-dependent processes. For example, SNF2H reacts to ADP β S with a sensitivity four times higher than CHD3 regarding the ATP hydrolysis activity, a tendency which we can also observe in preliminary experiments for ApCp (Fig. 4A and Figure S5a). Since ApCp and ADP β S are nucleotide analogues with modified α - and/or β -phosphate(s), our data would therefore offer a broad basis for developing ‘SNF2H-specific’ inhibitors. In addition, compared to CHD3, the nucleosome remodeling activity of SNF2H is

strongly affected by ADP (Figs 4B, 5B, 6B and Figure S5b,c and S6b). Since nucleotides do not inhibit the binding of both enzymes to nucleosomes (Figs S5d and S6c) and both enzymes exhibit comparable ADP IC $_{50}$ values in ATP hydrolysis assays (Fig. 4A) and enzymatic activities in general (Fig. 2 and Fig. S3), we propose that CHD3 requires less energy for nucleosome remodeling than SNF2H. This is in line with our remodeling data for both enzymes, which show that CHD3 can visibly translocate nucleosomes at much lower ATP concentrations compared to SNF2H (Fig. 2E and Fig. S3f). Finally, our nucleosome remodeling experiments of the CHD3 and SNF2H Q- and I-motif mutants also support this idea (Fig. 7C and Fig. S9). All mutants can still bind nucleosomes, exhibit comparable wild-type similar basal (nonstimulated) ATP hydrolysis rates, but fail to increase the ATPase hydrolysis rates in the presence of nucleosomes (Fig. 7B and Fig. S8), matching our previous results for BRG1 [Snf2 subfamily] [11]. But different to BRG1, three CHD3 (Q740A/E and K767R) variants and only the cancer-relevant SNF2H (D182N) Q-motif variant still allow a sufficient transfer of the released lower energy levels into nucleosome movement (Fig. 7C and Fig. S8). Even if the mutants would show slightly worse affinities to nucleosomes, which we admittedly cannot detect with the sensitivity of the IP approach, this would not satisfyingly explain the drastic breakdowns in ATPase hydrolysis rates and nucleosome remodeling activities (Fig. 7B,C and Fig. S9). Our findings therefore suggest that amino acid interactions, including the highly conserved Q- and K-residues, and/or conformational changes in the ATPase domains (Fig. 1 and Supplementary Fig. S1,2), play distinct regulatory roles in the ATPase-dependent functions of CHD3 and SNF2H, ultimately allowing a ‘more efficient coupling’ between ATP hydrolysis and nucleosome remodeling for CHD3, than for SNF2H (or for BRG1). Interestingly, similar observations, such as that ATP hydrolysis rate and remodeling activity do not necessarily have to correlate causally, have already been made for other remodeling enzymes. A mBRG1 E1083G (in the ATPase domain) variant reveals a reduced nucleosome remodeling activity, despite a normal ATPase activity [57]. On the other hand, yeast SWI/SNF [Snf2 subfamily] has been shown to exhibit a stimulated nucleosome mobilization activity in the presence of IP $_4$ and IP $_5$, without changes in the ATP hydrolysis rate [49].

Beside ADP, we have confirmed IP $_6$ as a further endogenous molecule that inhibits the remodeling activity of CHD3 and SNF2H (Fig. 6A,B and Fig. S6b). This is in agreement with the observations

made for hINO80 [Ino80 subfamily] by [51]. The inhibitory effect of IP₆ is already visible at concentrations of 0.5 mM (Fig. 6A,B and Fig. S6b), what is within the value range of the intracellular IP₆ concentrations (10 μM to 1 mM) [58–60]. Interestingly, IP₆ and its precursors play a role in various nuclear processes like transcriptional control, DNA repair, mRNA export, or chromatin remodeling [61–64]. IP₆ is a competitive inhibitor of CHD3, but IP₆ cannot be displaced from SNF2H by excess ATP (Figs 3, Fig. 6B,C and Fig. S4b). In this regard, it is interesting to note that Willhoft *et al.* [51] have proposed a noncompetitive IP₆ inhibition mode for INO80 with the putative IP₆ binding site between aa 487 and 1556 (including the bipartite ATPase domain). However, in contrast to our results for SNF2H, INO80 exhibits an almost 10 times reduced nucleosome binding affinity in the presence of 1 mM ATP and 250 μM IP₆ [51]. Even though our IP approach does not allow for a quantitative analysis, changes in this size range should be visible. Furthermore, we consider a reduced nucleosome affinity as the sole explanation for the drastically reduced remodeling activity as rather unlikely (see also above). Beyond that, our data also show that CHD3 and SNF2H can bind nucleotides and nucleosomes independently, indicating that the substrates tend not to influence the binding of the respective other substrate (Fig. 2A,B, Fig. 3, Fig. 5C, Fig. 6C, Fig. 7A and Supplementary Figs S4, 5d, 6c), as it has been already shown for BRG1 [11]. Although the inhibition mechanism for SNF2H has not been explored in detail, our results show that two remodelers from two subfamilies seem to be inhibited by IP₆ via different mechanisms, putatively including targeting of distinct protein domains. However, an amino acid alignment between SNF2H full length and the proposed IP₆ binding site of INO80 (Fig. S6a) reveals no significant sequence identity, except in the N-terminal half of the ATPase domain, which would open the possibility of a noncompetitive inhibitor that binds in the active side [65]. But of course other inhibitory modes such as competitive binding with IP₆ having higher affinity (so ATP cannot displace it) or mixed binding, where IP₆ binds both the ATPase domain and another domain, which is also affecting the enzymatic activity cannot be excluded.

Interestingly, the aspect of different binding sites of the ligands, tested in terms of this manuscript, becomes even apparent on a small scale, since the ‘IP₆-binding footprints’ in the ATPase domain of CHD3 differ in part from those generated by ADP (and ATP) (Fig. 3 and Fig. S4b). Moreover, in contrast to ADP, IP₆ causes structural changes, being reflected by regions of increased deuterium exchange (Fig. 3D and

Fig. S4b). Taken together, the data indicate that ADP and IP₆ perform competitive inhibition on ATPase-dependent processes of CHD3 by (i) partially different binding sites within the ATPase domain and/or (ii) different concomitant events such as ligand-specific structural rearrangements.

In line with our experiments, arguing for functional differences between CHD3 and SNF2H in ATPase-dependent activities, sequence alignments show minor, but characteristic differences in the ATPase domains of both enzymes (despite a high general sequence identity in this part) (Fig. 1B and Figs S1,2). Interestingly, ‘sequence insert 3’ colocalizes with a HDXMS peptide, covering amino acids 1040–1055 and showing exclusive ADP binding ‘footprints’ (Fig. 1B, Fig. 3A,D and Figs S1, 2, 4b (orange frame)). Furthermore, a cryo-EM study of hCHD4 that shares 71.6% identical residues with the homologous CHD3 [10] reveals that the counterpart of ‘sequence insert 3’ in CHD4 also contacts nucleosomal DNA [66]. Beyond that, some of the detected inserts align with parts of loops in our homology models of the ATPase domains of CHD3 and SNF2H (Fig. 1B and Fig. S1). Helicase-like enzymes undergo conformational changes upon ATP hydrolysis, comprising reorientations of both RecA-like domains relative to each other or of single ATPase domain parts [6,37,67]. Accordingly, we observe regions with increased deuterium exchange in- and outside of the ATPase domain, upon ATP binding (Fig. 3 and Fig. S4b, pink frame). Taken together, it is therefore conceivable that these sequence differences in the ATPase domains of CHD3 and SNF2H are a reason for the different/remodeler-specific behavior regarding various ATPase-dependent processes in the presence of inhibitory ligands or upon mutagenesis of conserved ATPase domain motifs.

Certainly, ‘subfamily-specific remodeler domains’ other than the ATPase domain may also account for the observed functional differences between CHD3 and SNF2H. However, studies of dISWI (i) [Iswi subfamily] and *S. cerevisiae* CHD1 (ii) [Chd1 subfamily] suggest that the ATPase domain rather represents the central and basic functional domain of these enzymes, being merely influenced by domains such as HSS (i) or Chromo- and DBD (ii) regarding template affinity and/or specificity or nucleosome positioning specificity [25,30,33,34]. Interestingly, the ATPase domain of ISWI even exhibits an autonomous nucleosome remodeling activity [34]. Since wild-type CHD3 and SNF2H exhibit comparable substrate affinities and enzymatic activities in general (Fig. 2 and Fig. S3), we therefore propose that the sequence differences in the ATPase domains of both remodelers mainly account

for the different functional results. This also implies that the ATPase domains are suited as targets for specific inhibitors. Accordingly, also Vangamudi and colleagues [23] have proposed the idea that the ATPase domain surpasses the Bromodomain (testing PFI-3 as a Bromodomain inhibitor) as drug target in SWI/SNF mutant cancers, since the Bromodomain function of SMARCA4 [Snf2 subfamily] has been found to be insubstantial for tumor cell proliferation, whereas the ATPase activity has been crucial. In our opinion, the presence of 'subfamily-specific accessory domains' could therefore possibly even help to achieve 'tailor made' (regulative) effects of ATPase targeted drugs for certain chromatin remodelers.

Beyond that, our data suggest that endogenous molecules such as ADP and IP₆ also regulate chromatin remodeling enzymes in living cells. Distinct nucleosome positioning properties have been ascribed to remodeling enzymes, arguing for a certain 'nucleosome barcoding system' generated by remodeling enzymes [10,20]. The differential *in vivo* regulation of remodeling enzymes by ADP or IP₆ would allow further fine tuning of this 'barcoding' in order to react specifically and individually to diverse physiological and pathological events like for example cancer, which is known to cause changes in the ATP/ADP ratio [68]. In mouse pancreatic beta cells, the ATP/ADP ratio rises from ~2–3 to ~8–9 upon glucose stimulation and decreases in ischemia from ~8 to ~0.4 [69–73]. Our experiments reveal remodeler subfamily differences in sensitivity to such ATP/ADP ratios *in vitro*, representing therefore a valid *in vitro* model to study the regulation of such enzymes upon changes in the ATP/ADP proportion (Figs 4–6 and Figs S5a–c, S6b). In this regard, it is interesting to note that initial attempts to deplete ATP upon sodium azide treatment in U2OS and HEK293T cells, indicate that SNF2L [Iswi subfamily] and SNF2H exhibit higher mobility and a lower percentage of chromatin immobilization in comparison with nontreated cells in FRAP and FCS experiments [74]. Furthermore, they show that the naturally occurring, ATPase-deficient SNF2L mutant (SNF2L +13: splice variant), exhibits higher diffusion coefficients and a lower immobile fraction than the SNF2L wild-type protein in control and ATP-depleted U2OS cells. On the other hand, ChIP experiments of Xie and coworkers [75] showed that the KR-mutant (motif I) of CHD4, a protein very similar to CHD3 [10], is binding as efficiently to the rDNA locus than the wild-type CHD4 protein. In line with the latter findings, our *in vitro* binding studies show that ADP, ATP γ S, or ADP β S or the mutagenesis of the highly conserved Q- and K-residues of the Q-motif and motif I do not

prevent CHD3 and SNF2H or their variants from binding to nucleosomes (see also above and Figs S5, 6c, 8). Remodeling enzymes normally act in the context of protein complexes in living cells [5], so teasing apart the differences between purified and cellular systems will require further studies. Looking at the experimental tools, currently available in chromatin research, the analysis of nucleosome translocation by a single remodeler in cells will be challenging, since most of the genomic loci are regulated and targeted by more than one remodeling enzyme [76].

Ultimately, our data strongly suggest the ATPase domain as a valuable target for endogenous regulation and deliver a promising basis to design more selective nucleoside and nucleotide analogues like ADP β S or ApCp and as well IP₆ derivatives in order to enable remodeler-specific ATPase targeting. Because nucleotide analogues are already widely used for treatments of cancer or Herpesvirus infections [77,78] and as IP₆ has an anticancer effects [79], such therapeutic approaches can be further investigated based on this pool of existing experience.

Materials and Methods

Nucleosome assembly

The nucleosome assembly strategy and procedure is described in detail in [10]. In brief, for the assembly of centrally (77-NPS-77/0-NPS-0) and end positioned (0-NPS-77) mononucleosomes, with 77 or 0 bp comprising linker DNA, primer combinations from [10] were used, in order to amplify the respective DNA sequences from a Bgl II digested and gel purified DNA fragment of pPCRScrip_t-slog1-gla75. In case of the biotin labeled, centrally (77-NPS-77) positioned nucleosomes, the reverse primer (GTACAGAGAGGGAGAGTCACAAAAC) was labeled at its 5'-end with biotin. In case of the Cy3-labeled 0-NPS-0 nucleosome, the reverse primer (TAGCTGTATATATCTGACACATG) was labeled at its 5'-end with Cy3. The PCR amplified NPS-sequence was Ethanol/NH₄-acetate precipitated and dissolved in water. The DNA template preparation for the nucleosome assembly of drosophila HSP70 promotor and -190/+90 mouse rDNA promotor can be found in [10]. The nucleosomes were generated by salt gradient dialysis, using chicken histone octamer (for preparation see also [10]): DNA ratios, varying from 0.5 : 1 to 1 : 1 [10]. The mononucleosome concentration was determined by dividing the amount of DNA, used for the assembly reaction, through the total reaction volume after dialysis. Circular pT11 plasmid DNA was assembled with human octamers (for preparation see also [10]) into circular chromatin as described above.

Electro mobility shift assay

For electro mobility shift assay (EMSA), we performed two biological replicates for CHD3 and SNF2H. Cy3-labeled 0-NPS-0 mononucleosomes (concentrations varied between 29.9–30.2 nM) were incubated with raising chromatin remodeler amounts (always 1 : 2 dilutions with 9–15 dilution steps; highest CHD3 concentrations: 620/798 nM; highest SNF2H concentrations: 2710/2810 nM; see also Fig. 2C).

As a control, one sample only contained nucleosomes without remodeler. The assays were performed for 20 min at 30 °C in 20 mM T

ris/HCl pH 7.6/ 120 mM KCl/ 1.5 mM MgCl₂/0.5 mM EGTA/200–300 ng/μL BSA (total reaction volume 10 μL). The binding reactions were subsequently supplemented with 1–2 μL 50% glycerol and loaded on 6% PAA gels, which were scanned on a Fluorescence Image Reader

FLA-3000 (Fujifilm Holdings Corporation, Tokyo, Japan). The intensity decrease of the initial nucleosome band with increasing remodeler concentrations was quantified via ImageJ and plotted over the remodeling enzyme concentration in SigmaPlot13.0.

These data were subsequently fitted to the Hill equation.

Nucleosome remodeling reaction

Nucleosome remodeling assays were performed in 20 mM Tris/HCl pH 7.6/80–150 mM KCl/1.5 mM MgCl₂/0.5 mM EGTA/10% Glycerol/1 μM–1 mM ATP in the presence or absence of ADP, various nucleotide analogues, IP₆ and IP₆ precursors (concentrations and molecule names are given in the respective assays) at 30 °C for 60 min (in some assays the total incubation time was 2 h, which is indicated in the respective figure) in ~ 10–11 μL reaction volume (for remodeling assays with inositol phosphates MgCl₂ was adjusted to 2.5 mM). Each reaction contained mononucleosomes in concentrations of 80 or 120–135 nM (77-NPS-77 or 0-NPS-77) or 37–44 ng/μL (drosophila HSP70 promotor and –190/+90 mouse rDNA promotor). The final concentration of recombinant nucleosome remodeling enzymes varied from 25 to 500 nM. The enzymatic reactions were stopped by adding 300–1000 ng competitor (plasmid) DNA for 5 min at 30 °C. The nucleosome movements were visualized, by supplementing the reactions with glycerol (4–5%) and loading them on 5% or 6% native 0.4x TBE PAA gels, which were subsequently stained with ethidium bromide.

ATP filter binding assay

To assay ATP binding 200 nM of CHD3, SNF2H or their respective mutants were mixed with 0,375 μCi (13.88 kBq) [γ -³²P]-ATP (corresponding to 82–165 nM) in 20 mM HEPES pH 7.6/2.8 mM MgCl₂/120 mM KCl/0.4 mM EDTA/10% Glycerol. Nonradioactive ATP, ADP, GTP and IP₆ were added as need in a range from 1 μM to 1 mM. The volume was

adjusted to 15 μL and the reactions incubated for 30 min at 30 °C. A 45-mm-diameter piece of 0.45-μm nitrocellulose membrane was installed in a vacuum filtration system and washed with 20 mL buffer A (20 mM HEPES pH 7.6/100 mM KCl/0.4 mM EDTA/10% Glycerol). In total, 16 times 5 μL of the binding reactions was spotted on the nitrocellulose membrane under vacuum and the membrane was washed with 150 mL of buffer A. The membrane was dried at 65 °C immediately afterward and placed on a phosphoimager screen. After exposure, overnight screens were read out on a Typhoon FLA 9500 imager. Bound [γ -³²P]-ATP was quantified in Fuji-Film Multi Gauge 3.0. Averages and standard deviations were calculated in Microsoft Excel.

Radioactive ATPase-assay

Recombinantly purified CHD3, SNF2H, and their respective mutants (40–250 nM) were incubated with 130 nM 77-NPS-77 mononucleosomes in 20 mM Tris/HCl pH 7.6/120 mM KCl/1.5 mM MgCl₂/0.5 mM EGTA/10% glycerol in the presence of 8–600 μM ATP and 0.1 μCi [γ -³²P]-ATP for 40 min at 30 °C. Released ³²P_i was separated from non-hydrolyzed [γ -³²P]-ATP by TLC on PEI-Cellulose F plates (Merck) [mobile phase: 50% acetic acid, 0.5 mM LiCl]. ³²P_i to [γ -³²P]-ATP ratios were calculated after phosphoimaging (Typhoon FLA 9500), using Fuji Multi Gauge Software and Excel. Concentration of hydrolyzed ATP was calculated from these ratios and the (total) initial ATP concentration in the assay. *K_m* values for CHD3 and SNF2H with and without ADP (10 and 20 μM) were obtained from ATPase assays done with varying concentrations of non-radioactive ATP (8–600 μM) and a constant 0.1 μCi of [γ -³²P]-ATP. ATPase rates were fitted to the Michaelis-Menten equation using SigmaPlot version 13.0. Inhibition of remodeling enzymes was tested by using the assay described above with a fixed concentration of 125 μM non-radioactive ATP and 0.1 μCi [γ -³²P]-ATP, supplemented with varying concentrations of inhibitor (2–1000 μM). Averages and standard deviations for the ATPase rates represent three experiments, done with two to three independent protein preparations. To determine IC₅₀ values, the ATPase rate was plotted as a function of the inhibitor concentration and fitted to the Hill Equation in Sigma Plot 13.0. This fit yields also the Hill coefficient, in addition to the IC₅₀-value. ATPase assays to test for mutant ATPase activity were done with the conditions described above at 0.5 mM ATP and with the remodeler concentrations indicated at the individual experiments.

Hydrogen/deuterium exchange mass spectrometry

Hydrogen/deuterium exchange mass spectrometry (HDXMS) was performed using a Waters Synapt G2Si

equipped with nanoACQUITY UPLC system with H/DX technology and a LEAP autosampler. The final concentration of protein in each sample was 5 μM in the absence or presence of 1 mM ADP, ATP, or IP₆. For each deuteration time, 4 μL complex was mixed with 56 μL D₂O buffer (25 mM Tris pH 7.5, 150 mM NaCl, 1 mM DTT, 0.5 mM EDTA, \pm 1 mM ADP, ATP, or IP₆ in D₂O) for 0, 0.5, 1, 2, or 5 min at 25 °C. The exchange was quenched with an equal volume of quench solution (3 M guanidine, 0.1% formic acid, pH 2.66). The quenched sample (50 μL) was injected into the sample loop, followed by digestion on an in-line pepsin column (immobilized pepsin, Pierce, Inc., Thermo Scientific Pierce, Rockford, IL, USA) at 15 °C. The resulting peptides were captured on a BEH C18 Vanguard precolumn, separated by analytical chromatography (Acquity UPLC BEH C18, 1.7 μm , 1.0 X 50 mm, Waters Corporation, Milford, MA, USA) using a 7–85% acetonitrile in 0.1% formic acid over 7.5 min, and electrosprayed into the Waters SYNAPT G2Si quadrupole time-of-flight mass spectrometer. The mass spectrometer was set to collect data in the Mobility, ESI+ mode; mass acquisition range of 200–2000 (m/z); scan time 0.4 s. Continuous lock mass correction was accomplished with infusion of leu-enkephalin (m/z = 556.277) every 30 s (mass accuracy of 1 ppm for calibration standard). For peptide identification, the mass spectrometer was set to collect data in MS^E, Mobility-ESI+ mode instead and twice as much protein was injected. The peptides were identified from triplicate MS^E analyses, and data were analyzed using PLGS 2.5 (Waters Corporation). Peptide masses were identified using a minimum number of 250 ion counts for low energy peptides and 50 ion counts for their fragment ions. The peptides identified in PLGS were then analyzed in DynamX 3.0 (Waters Corporation). Because the protein was so large (2000 amino acids), the ion mobility times provided critical information along with retention time and parent ion mass for resolving overlaps to confidently identify the peptides in the DynamX 3.0 software. The relative deuterium uptake for each peptide was calculated by comparing the centroids of the mass envelopes of the deuterated samples vs. the undeuterated controls following previously published methods [80] and corrected for back-exchange as previously described [45]. The experiments were performed in triplicate, and independent replicates of the triplicate experiment were performed to verify the results.

Generation of multiple sequence alignments and differential logos

For the two remodelers CHD3 (UniProt-ID Q12873) and SNF2H (UniProt-ID O60264), the UniRef 90% identity sequence sets were deduced from the UniProt database (release 2017_09) and aligned. These two remodeler-specific multiple sequence alignments (MSAs) were manually curated by means of Jalview [81] to eliminate outliers

like strikingly short sequences. These datasets contained 275 and 196 sequences, respectively. For the identification of indels, sequences were merged and realigned by means of MAFFT [82] as implemented in Jalview. This final MSA is given in Fig. S2; it was used to create a differential sequence logo by means of cSeqLogo (<https://www.bioinf.ur.de/>). This is an in-house program using the WebLogo 3 library [83] to create a two-sample sequence logo highlighting the similarities and differences of both sequence sets.

Acknowledgements

Dr. Josef Exler for kindly providing us with the pENTRY- and pDEST-vectors and the virus for hSNF2H WT. Dr. Sophia Pinz for kindly providing us with the pDFBC-His CHD3 vector and the respective virus. Maria Theresia Watzlowik for providing us with chromatin assembled pT11 DNA. Elisabeth Silberhorn and Dr. Rodrigo Maldonado for providing help with cloning, and Christine Lemche–Auerbach for purifying proteins. Several practical trainees: Maria Engelhart: purifying proteins; Katja Brandl: for cloning and virus production; Benedict Cramer: virus production; Nicole Spitzberger: virus production. We also want to thank Dr. Sandra Schlee, Dr. Patrick Babinger, and Klaus Tiefenbach (University of Regensburg) for advices in Sigma Plot and data analysis. This work was supported by a grant (SFB 960) from the Deutsche Forschungsgesellschaft (DFG).

Conflict of interest

The authors declare no conflict of interest.

Author contributions

HH, AF, EK, JN, LH, RM, and SD performed the experimental design. HH, AF, EK, JN, LH, LS, and RGF involved in performance of experiments. HH, AF, EK, JN, LH, and RM performed the experimental analysis. HH, AF, EK, RM, SD, and GL wrote the manuscript. GL performed the financing of the study.

Peer Review

The peer review history for this article is available at <https://publons.com/publon/10.1111/febs.15699>.

References

- 1 Huang RC & Bonner J (1965) Histone-bound RNA, a component of native nucleohistone. *Proc Natl Acad Sci U S A*. **54**, 960–967.

- 2 Rodríguez-Campos A & Azorín F (2007) RNA Is an integral component of chromatin that contributes to its structural organization. *PLoS ONE* **2**, e1182.
- 3 Bannister AJ & Kouzarides T (2011) Regulation of chromatin by histone modifications. *Cell Res* **21**, 381–395.
- 4 Breiling A & Lyko F (2015) Epigenetic regulatory functions of DNA modifications: 5-methylcytosine and beyond. *Epi Chromat* **8**, 24.
- 5 Clapier CR & Cairns BR (2009) The biology of chromatin remodeling complexes. *Annu Rev Biochem* **78**, 273–304.
- 6 Flaus A, Martin DMA, Barton GJ & Owen-Hughes T (2006) Identification of multiple distinct Snf2 subfamilies with conserved structural motifs. *Nucleic Acids Res* **34**, 2887–2905.
- 7 Seelig HP, Moosbrugger I, Ehrfeld H, Fink T, Renz M & Genth E (1995) The major dermatomyositis-specific Mi-2 autoantigen is a presumed helicase involved in transcriptional activation. *Arthritis Rheum* **38**, 1389–1399.
- 8 Wong AK, Shanahan F, Chen Y, Lian L, Ha P, Hendricks K, *et al.* (2000) BRG1, a component of the SWI-SNF complex, is mutated in multiple human tumor cell lines. *Cancer Res* **60**, 6171–6177.
- 9 Kovač K, Sauer A, Maćinković I, Awe S, Finkernagel F, Hoffmeister H, *et al.* (2018) Tumour-associated missense mutations in the dMi-2 ATPase alters nucleosome remodelling properties in a mutation-specific manner. *Nat Commun* **9**, 2112.
- 10 Hoffmeister H, Fuchs A, Erdel F, Pinz S, Gröbner-Ferreira R, Bruckmann A, *et al.* (2017) CHD3 and CHD4 form distinct NuRD complexes with different yet overlapping functionality. *Nucleic Acids Res* **45**, 10534–10554.
- 11 Hoffmeister H, Fuchs A, Strobl L, Sprenger F, Gröbner-Ferreira R, Michaelis S, *et al.* (2019) Elucidation of the functional role of the Q- and I-motif in the human chromatin remodeling enzyme BRG1. *J Biol Chem* **294**, 3294–3310.
- 12 Le Gallo M, O'Hara AJ, Rudd ML, Urlick ME, Hansen NF, O'Neil NJ, *et al.* (2012) Exome sequencing of serous endometrial tumors identifies recurrent somatic mutations in chromatin-remodeling and ubiquitin ligase complex genes. *Nat Genet* **44**, 1310–1315.
- 13 Stopka T, Zakova D, Fuchs O, Kubrova O, Blafkova J, Jelinek J, *et al.* (2000) Chromatin remodeling gene SMARCA5 is dysregulated in primitive hematopoietic cells of acute leukemia. *Leukemia* **14**, 1247–52.
- 14 Prasad P, Lennartsson A & Ekwall K (2015) The roles of SNF2/SWI2 nucleosome remodeling enzymes in blood cell differentiation and leukemia. *BioMed Res Int* **2015**, e347571.
- 15 Wang Y, Qin J, Liu Q, Hong X, Li T, Zhu Y, *et al.* (2016) SNF2H promotes hepatocellular carcinoma proliferation by activating the Wnt/ β -catenin signaling pathway. *Oncol Lett* **12**, 1329–1336.
- 16 Chu X, Guo X, Jiang Y, Yu H, Liu L, Shan W, *et al.* (2017) Genotranscriptomic meta-analysis of the CHD family chromatin remodelers in human cancers – initial evidence of an oncogenic role for CHD7. *Mol Oncol* **11**, 1348–1360.
- 17 Bouazoune K & Brehm A (2005) dMi-2 chromatin binding and remodeling activities are regulated by dCK2 phosphorylation. *J Biol Chem* **280**, 41912–41920.
- 18 Klinker H, Mueller-Planitz F, Yang R, Forné I, Liu C-F, Nordenskiöld L, *et al.* (2014) ISWI remodelling of physiological chromatin fibres acetylated at lysine 16 of histone H4. *PLoS ONE* **9**, e88411.
- 19 Eberharder A & Becker PB (2004) ATP-dependent nucleosome remodelling: factors and functions. *J Cell Sci* **117** (Pt 17), 3707–3711.
- 20 Rippe K, Schrader A, Riede P, Strohnner R, Lehmann E & Langst G (2007) DNA sequence- and conformation-directed positioning of nucleosomes by chromatin-remodeling complexes. *Proc Natl Acad Sci U S A* **104**, 15635–15640.
- 21 Goodarzi AA, Kurka T & Jeggo PA (2011) KAP-1 phosphorylation regulates CHD3 nucleosome remodeling during the DNA double-strand break response. *Nat Struct Mol Biol* **18**, 831–839.
- 22 Filippakopoulos P & Knapp S (2014) Targeting bromodomains: epigenetic readers of lysine acetylation. *Nat Rev Drug Discov* **13**, 337–356.
- 23 Vangamudi B, Paul TA, Shah PK, Kost-Alimova M, Nottebaum L, Shi X, *et al.* (2015) The SMARCA2/4 ATPase domain surpasses the bromodomain as a drug target in SWI/SNF mutant cancers: Insights from cDNA rescue and PFI-3 inhibitor studies. *Cancer Res* **75**, 3865–3878.
- 24 Marfella CGA & Imbalzano AN (2007) The Chd family of chromatin remodelers. *Mutat Res* **618**, 30–40.
- 25 Grüne T, Brzeski J, Eberharder A, Clapier CR, Corona DFV, Becker PB, *et al.* (2003) Crystal structure and functional analysis of a nucleosome recognition module of the remodeling factor ISWI. *Mol Cell* **12**, 449–460.
- 26 Silva APG, Ryan DP, Galanty Y, Low JKK, Vandevenne M, Jackson SP, *et al.* (2015) The N-terminal region of CHD4 is essential for activity and contains a HMG-box-like-domain that can bind poly (ADP-ribose). *J Biol Chem* **291**, 924–938.
- 27 Thomä NH, Czyzewski BK, Alexeev AA, Mazin AV, Kowalczykowski SC & Pavletich NP (2005) Structure of the SWI2/SNF2 chromatin-remodeling domain of eukaryotic Rad54. *Nat Struct Mol Biol* **12**, 350–356.
- 28 Dürr H, Körner C, Müller M, Hickmann V & Hopfner K-P (2005) X-ray structures of the Sulfolobus

- solftaricus SWI2/SNF2 ATPase core and its complex with DNA. *Cell* **121**, 363–373.
- 29 Shaw G, Gan J, Zhou YN, Zhi H, Subburaman P, Zhang R, et al. (2008) Structure of RapA, a Swi2/Snf2 protein that recycles RNA polymerase during transcription. *Struct Lond Engl* **16**, 1417–1427.
- 30 Hauk G, McKnight JN, Nodelman IM & Bowman GD (2010) The chromodomains of the Chd1 chromatin remodeler regulate DNA access to the ATPase motor. *Mol Cell* **39**, 711–723.
- 31 Hauk G & Bowman GD (2011) Structural insights into regulation and action of SWI2/SNF2 ATPases. *Curr Opin Struct Biol* **21**, 719–727.
- 32 Sundaramoorthy R, Hughes AL, Singh V, Wiechens N, Ryan DP, El-Mkami H, et al. (2017) Structural reorganization of the chromatin remodeling enzyme Chd1 upon engagement with nucleosomes. *eLife*;6: e22510.
- 33 McKnight JN, Jenkins KR, Nodelman IM, Escobar T & Bowman GD (2011) Extranucleosomal DNA binding directs nucleosome sliding by Chd1. *Mol Cell Biol*. **31**, 4746–4759.
- 34 Mueller-Planitz F, Klinker H, Ludwigsen J & Becker PB (2013) The ATPase domain of ISWI is an autonomous nucleosome remodeling machine. *Nat Struct Mol Biol* **20**, 82–89.
- 35 Tanner NK, Cordin O, Banroques J, Doère M & Linder P (2003) The Q motif: a newly identified motif in DEAD box helicases may regulate ATP binding and hydrolysis. *Mol Cell* **11**, 127–138.
- 36 Rocak S & Linder P (2004) DEAD-box proteins: the driving forces behind RNA metabolism. *Nat Rev Mol Cell Biol* **5**, 232–241.
- 37 Ye J, Osborne AR, Groll M & Rapoport TA (2004) RecA-like motor ATPases – lessons from structures. *Biochim Biophys Acta* **1659**, 1–18.
- 38 Logie C & Peterson CL (1999) Purification and biochemical properties of yeast SWI/SNF complex. *Methods Enzymol* **304**, 726–741.
- 39 Wang HB & Zhang Y (2001) Mi2, an auto-antigen for dermatomyositis, is an ATP-dependent nucleosome remodeling factor. *Nucleic Acids Res* **29**, 2517–2521.
- 40 Smith CL & Peterson CL (2005) A conserved Swi2/Snf2 ATPase motif couples ATP hydrolysis to chromatin remodeling. *Mol Cell Biol* **25**, 5880–5892.
- 41 Aalfs JD, Narlikar GJ & Kingston RE (2001) Functional Differences between the Human ATP-dependent nucleosome remodeling proteins BRG1 and SNF2H. *J Biol Chem* **276**, 34270–34278.
- 42 Milo R & Phillips R (2015) Cell Biology by the Numbers [Internet], 1st edn.. GS Garland Science Taylor & Francis Group, New York, NY. [cited 2018 Jan 22]. 358 pages | 181 illustrations. Available from: <http://garlandscience.com/product/isbn/9780815345374>.
- 43 Tantama M, Martínez-François JR, Mongeon R & Yellen G. Imaging energy status in live cells with a fluorescent biosensor of the intracellular ATP-to-ADP ratio. *Nat Commun* [Internet]. 2013 Oct 7 [cited 2014 Jul 15]; 4. Available from: <http://www.nature.com/ncomms/2013/131007/ncomms3550/full/ncomms3550.html>.
- 44 Rippe K, Schrader A, Riede P, Strohner R, Lehmann E & Langst G (2007) DNA sequence- and conformation-directed positioning of nucleosomes by chromatin-remodeling complexes. *Proc Natl Acad Sci U S A* **104**, 15635–15640.
- 45 Ramsey KM, Dembinski HE, Chen W, Ricci CG & Komives EA (2017) DNA and IκBα both induce long-range conformational changes in NFκB. *J Mol Biol* **429**, 999–1008.
- 46 Hafenbradl D, Baumann M & Neumann L. In vitro characterization of small-molecule kinase inhibitors. In: Klebl B, Müller G, Hamacher M, editors. Protein Kinases as Drug Targets [Internet]. Wiley-VCH Verlag GmbH & Co. KGaA; 2011 [cited 2017 Feb 21]. p. 1–43. Available from: <http://onlinelibrary.wiley.com/doi/10.1002/9783527633470.ch1/summary>.
- 47 Ellington WR (1989) Phosphocreatine represents a thermodynamic and functional improvement over other muscle phosphagens. *J Exp Biol* **143**, 177–194.
- 48 Biswas S, Kinbara K, Niwa T, Taguchi H, Ishii N, Watanabe S, et al. (2013) Biomolecular robotics for chemomechanically driven guest delivery fuelled by intracellular ATP. *Nat Chem* **5**, 613–620.
- 49 Shen X, Xiao H, Ranallo R, Wu W-H & Wu C (2003) Modulation of ATP-dependent chromatin-remodeling complexes by inositol polyphosphates. *Science* **299**, 112–114.
- 50 Steger DJ, Haswell ES, Miller AL, Wente SR & O'Shea EK (2003) Regulation of chromatin remodeling by inositol polyphosphates. *Science* **299**, 114–116.
- 51 Willhoft O, Bythell-Douglas R, McCormack EA & Wigley DB (2016) Synergy and antagonism in regulation of recombinant human INO80 chromatin remodeling complex. *Nucleic Acids Res* **44**, 8179–8188.
- 52 de Frutos M, Raspaud E, Leforestier A & Livolant F (2001) Aggregation of nucleosomes by divalent cations. *Biophys J* **81**, 1127–1132.
- 53 Wu Y, Sommers JA, Loiland JA, Kitao H, Kuper J, Kisker C, et al. (2012) The Q motif of Fanconi Anemia Group J Protein (FANCI) DNA helicase regulates its dimerization, DNA binding, and DNA repair function. *J Biol Chem* **287**, 21699–21716.
- 54 Nongkhaw M, Dutta P, Hockensmith JW, Komath SS & Muthuswami R (2009) Elucidating the mechanism of DNA-dependent ATP hydrolysis mediated by DNA-dependent ATPase A, a member of the SWI2/SNF2 protein family. *Nucleic Acids Res* **37**, 3332.

- 55 Nongkhlaw M, Gupta M, Komath SS & Muthuswami R (2012) Motifs Q and I are required for ATP hydrolysis but not for ATP binding in SWI2/SNF2 proteins. *Biochemistry* **51**, 3711–3722.
- 56 Forbes SA, Beare D, Boutselakis H, Bamford S, Bindal N, Tate J, *et al.* (2017) COSMIC: somatic cancer genetics at high-resolution. *Nucleic Acids Res* **45**, D777–D783.
- 57 Bultman S, Gebuhr T, Yee D, La Mantia C, Nicholson J, Gilliam A, *et al.* (2000) A Brg1 null mutation in the mouse reveals functional differences among mammalian SWI/SNF complexes. *Mol Cell* **6**, 1287–1295.
- 58 French PJ, Bunce CM, Stephens LR, Lord JM, McConnell FM, Brown G, *et al.* (1991) Changes in the levels of inositol lipids and phosphates during the differentiation of HL60 promyelocytic cells towards neutrophils or monocytes. *Proc Biol Sci* **245**, 193–201.
- 59 Shamsuddin AM (1999) Metabolism and cellular functions of IP6: a review. *Anticancer Res* **19**, 3733–3736.
- 60 Shamsuddin AK & Bose S (2012) IP6 (Inositol Hexaphosphate) as a signaling molecule. *Curr Signal Transduct Ther* **7**, 289–304.
- 61 York JD, Odom AR, Murphy R, Ives EB & Wente SR (1999) A phospholipase C-dependent inositol polyphosphate kinase pathway required for efficient messenger RNA export. *Science* **285**, 96–100.
- 62 Hanakahi LA, Bartlett-Jones M, Chappell C, Pappin D & West SC (2000) Binding of inositol phosphate to DNA-PK and stimulation of double-strand break repair. *Cell* **102**, 721–729.
- 63 Odom AR, Stahlberg A, Wente SR & York JD (2000) A role for nuclear inositol 1,4,5-trisphosphate kinase in transcriptional control. *Science* **287**, 2026–2029.
- 64 Shears SB (2000) Transcriptional regulation: a new dominion for inositol phosphate signaling? *BioEssays* **22**, 786–789.
- 65 Blat Y (2010) Non-competitive inhibition by active site binders. *Chem Biol Drug Des* **75**, 535–540.
- 66 Farnung L, Ochmann M & Cramer P (2019) Nucleosome-CHD4 chromatin remodeler structure explains human disease mutations. *bioRxiv* 665562.
- 67 Singleton MR & Wigley DB (2002) Modularity and specialization in superfamily 1 and 2 helicases. *J Bacteriol* **184**, 1819–1826.
- 68 Maldonado EN & Lemasters JJ (2014) ATP/ADP ratio, the missed connection between mitochondria and the warburg effect. *Mitochondrion* **19PA**:78–84.
- 69 DeVivo DC, Leckie MP, Ferrendelli JS & McDougal DB (1978) Chronic ketosis and cerebral metabolism. *Ann Neurol* **3**, 331–337.
- 70 Folbergrová J, Minamisawa H, Ekholm A, Siesjö BK. Phosphorylase a and labile metabolites during anoxia: correlation to membrane fluxes of K⁺ and Ca²⁺. *J Neurochem* **55**: 1690–1696.
- 71 Erecińska M & Silver IA (1994) Ions and energy in mammalian brain. *Prog Neurobiol* **43**, 37–71.
- 72 Nilsson T, Schultz V, Berggren PO, Corkey BE & Tornheim K (1996) Temporal patterns of changes in ATP/ADP ratio, glucose 6-phosphate and cytoplasmic free Ca²⁺ in glucose-stimulated pancreatic beta-cells. *Biochem J* **314** (Pt 1), 91–94.
- 73 Berg J, Hung YP & Yellen G (2009) A genetically encoded fluorescent reporter of ATP:ADP ratio. *Nat Methods* **6**, 161–166.
- 74 Erdel F, Schubert T, Marth C, Längst G & Rippe K (2010) Human ISWI chromatin-remodeling complexes sample nucleosomes via transient binding reactions and become immobilized at active sites. *Proc Natl Acad Sci U S A* **107**, 19873–19878.
- 75 Xie W, Ling T, Zhou Y, Feng W, Zhu Q, Stunnenberg HG, *et al.* (2012) The chromatin remodeling complex NuRD establishes the poised state of rRNA genes characterized by bivalent histone modifications and altered nucleosome positions. *Proc Natl Acad Sci U S A* **109**, 8161–8166.
- 76 Morris SA, Baek S, Sung M-H, John S, Wiench M, Johnson TA, *et al.* (2014) Overlapping chromatin-remodeling systems collaborate genome wide at dynamic chromatin transitions. *Nat Struct Mol Biol* **21**, 73–81.
- 77 Galmarini CM, Mackey JR & Dumontet C (2002) Nucleoside analogues and nucleobases in cancer treatment. *Lancet Oncol* **3**, 415–424.
- 78 Krečmerová M. Nucleoside and Nucleotide Analogues for the Treatment of Herpesvirus Infections: Current Stage and New Prospects in the Field of Acyclic Nucleoside Phosphonates. 2012 [cited 2018 Feb 7]; Available from: <http://www.intechopen.com/books/herpesviridae-a-look-into-this-unique-family-of-viruses/nucleoside-and-nucleotide-analogues-for-the-treatment-of-herpesvirus-infections-current-stage-and-ne>
- 79 Vucenik I & Shamsuddin AM (2003) Cancer inhibition by inositol hexaphosphate (IP6) and inositol: from laboratory to clinic. *J Nutr* **133** (11 Suppl 1), 3778S–3784S.
- 80 Wales TE, Fadgen KE, Gerhardt GC & Engen JR (2008) High-speed and high-resolution UPLC separation at zero degrees Celsius. *Anal Chem* **80**, 6815–6820.
- 81 Waterhouse AM, Procter JB, Martin DMA, Clamp M & Barton GJ (2009) Jalview Version 2—a multiple sequence alignment editor and analysis workbench. *Bioinforma Oxf Engl* **25**, 1189–1191.
- 82 Katoh K & Standley DM (2013) MAFFT multiple sequence alignment Software version 7: improvements in performance and usability. *Mol Biol Evol* **30**, 772–780.

- 83 Crooks GE, Hon G, Chandonia J-M & Brenner SE (2004) WebLogo: A sequence logo generator. *Genome Res* **14**, 1188–1190.
- 84 Walker JE, Saraste M, Runswick MJ & Gay NJ (1982) Distantly related sequences in the alpha- and beta-subunits of ATP synthase, myosin, kinases and other ATP-requiring enzymes and a common nucleotide binding fold. *EMBO J* **1**, 945–951.

Supporting information

Additional supporting information may be found online in the Supporting Information section at the end of the article.

File S1. 3D model of the ATPase domain from CHD3 and SNF2H.

File S2. Multiple sequence alignment (MSA) for CHD3 and SNF2H (see also separately attached file: Supplement 2 MSA CHD3_SNF2H_ref90.fa).

File S3. Supplementary experiments for the comparative analysis of CHD3 and SNF2H regarding their enzymatic activities.

File S4. HDXMS for CHD3.

File S5. Supplementary experiments regarding ATP hydrolysis rates and nucleosome remodeling of CHD3 and SNF2H in the presence of ADP.

File S5. Supplementary experiments regarding ATP hydrolysis rates and nucleosome remodeling of CHD3 and SNF2H in the presence of ADP.

File S6. Nucleosome binding- and remodeling experiments for CHD3 and SNF2H in the presence of IP₆ and amino acid alignment of human SNF2h and INO80.

File S7. CHD3 and SNF2H wild type and their respective mutants resolved on denaturing or native gels and nucleosome remodeling test for CHD3-C-His.

File S8. Nucleosome binding experiments for CHD3 and SNF2H and their respective mutants.

File S9. Nucleosome remodeling assays for Q-motif and motif I variants of CHD3 and SNF2H on 77-NPS-77 nucleosomes.

File S10. Supplementary Material and Methods.